Fluid history related to the early Eocene-middle Miocene convergent system of the Northern Apennines (Italy): Constraints from structural

JOURNAL OF GEOPHYSICAL RESEARCH, VOL. 115, B05405, doi:10.1029/2009JB006590, 2010

Fluid history related to the early Eocene-middle Miocene convergent system of the Northern Apennines (Italy): Constraints from structural and isotopic studies

Paola Vannucchi,[1] Francesca Remitti,[2] Giuseppe Bettelli,[2] Chiara Boschi,[3] and Luigi Dallai[3]

Received 4 May 2009; revised 16 November 2009; accepted 28 December 2009; published 25 May 2010.

[1] The late Eocene-middle Miocene erosive plate boundary between the European and the Adriatic plates is exhumed in the Northern Apennines of Italy. The fossil fault zone is 500 m thick and the outcropping portion exposes the first 5 km of its depth. At this plate boundary basal and frontal tectonic erosion incorporated unlithified, fluid-rich sediments into the fault zone. The deformation and nature of the material along the plate boundary define a fossil subduction channel. Here we couple a detailed structural analysis of the Apennine subduction channel, focusing, in particular, on calcite veins, with a stable isotope analysis to characterize the fluid regime along an active subduction channel. The ^{13}C and ^{18}O composition of calcite vein and host rock samples within the fault zone indicates that there is a deep metamorphic source of fluids migrating upward along the subduction channel, in addition to locally derived fluid components. Dewatering of subducting turbidites contributes significantly only in the shallowest part of the channel. Structural observations indicate fluid flow along and across the subduction channel. At deep levels fluid flow is associated with discrete deformation events on shear faults offset by dilational jogs filled with implosion breccias. At intermediate levels deformation is still cyclic and associated with repeated crack-and-seal events. At the shallowest levels deformation occurred, while portions of the subducting material were still unlithified. Here the deformation was quasicontinuous, without associated vein development. Both isotope and structural analyses indicate that this erosive subduction channel behaved as a weak fault with a vertical maximum principal stress.

Citation: Vannucchi, P., F. Remitti, G. Bettelli, C. Boschi, and L. Dallai (2010), Fluid history related to the early Eocene-middle Miocene convergent system of the Northern Apennines (Italy): Constraints from structural and isotopic studies, *J. Geophys. Res.*, *115*, B05405, doi:10.1029/2009JB006590.

1. Introduction

[2] The mechanics of the subduction megathrust plays a central role in tectonic processes shaping convergent margins. Understanding the mechanical behavior of subduction megathrusts is intimately tied to understanding their fluid regime.

[3] Convergent margins are particularly rich in migrating fluids that come from compacting sediments and dehydration reactions in subducting minerals [*Brown et al.*, 2001; *Saffer*, 2003; *Spinelli and Underwood*, 2004; *Screaton and Saffer*, 2005; *Saffer et al.*, 2008]. Most fluid drains along the plate boundary and from the plate boundary into the fractured upper plate [*Moore and Vrolijk*, 1992; *Carson and Screaton*, 1998; *Ranero et al.*, 2008]. It is an open question whether the mechanical and fluid characteristics of the plate boundary differ in significant ways between erosive and accretionary subduction zones. Both types of margins appear to be characterized by extension, that is, subvertical maximum principal stress, along their shallow portions, as confirmed by observations in modern subduction zones [*Sage et al.*, 2004; *Vannucchi and Leoni*, 2007; *Lewis et al.*, 2008]. In accretionary prisms the plate boundary megathrust cuts through the subducting plate, transferring material to the overriding plate. The subducting plate is generally rich in sedimentary layers whose main components are low-strength clays and in which faults preferentially develop [*Deng and Underwood*, 2001; *Underwood*, 2002]. At erosive margins the plate boundary migrates toward the overriding plate, removing material. The overriding plate is generally formed by strong, lithified rocks, especially compared to the subducting sediments, and the plate boundary megathrust appears to cut through high-strength material [*Vannucchi et al.*, 2001].

[1]Earth Science Department, University of Florence, Florence, Italy.
[2]Earth Science Department, University of Modena and Reggio Emilia, Modena, Italy.
[3]IGG-CNR, Pisa, Italy.

0148-0227/10/2009JB006590

[4] Proposed erosional mechanisms have been mostly inferred from indirect geophysical measurements [*Hilde*, 1983; *von Huene and Ranero*, 2003; *Ranero et al.*, 2008]. While some hypotheses imply mechanical scraping of the base of the overriding plate [*Hilde*, 1983], others support the primary action of migrating fluids through development of a high fluid pressure and hydrofracture of the upper plate [*Le Pichon et al.*, 1993; *von Huene et al.*, 2004]. Detailed geophysical [*Ranero et al.*, 2008] and field [*Vannucchi et al.*, 2008] studies have revealed strong coupling between the history of deformation and the fluid regime within erosive subduction boundaries.

[5] Despite the progress in understanding the similarities and differences between erosive and accretionary convergent margins [*Clift and Vannucchi*, 2004], many basic questions remain. For example, is the megathrust a zone of persistent along-fault fluid flow at erosive margins, as has been inferred from seismic measurements at the accretionary Barbados [*Bangs et al.*, 1999] and Nankai [*Bangs et al.*, 2004] margins? If present, do the fluids come from compaction or from deeper dehydration reactions at temperatures >150°C? How does deformation in the megathrust change as the rocks become increasingly lithified? What is the role of fluids in the megathrust earthquake cycle [*Ranero et al.*, 2008; *Audet et al.*, 2009]? What are the changes in the state of stress during this cycle? and Are these changes independent of depth, or is there a strong link between the cycle and the updip limit of the seismogenic zone?

[6] In this study we couple a detailed structural analysis of the veins inside the erosive plate boundary exhumed in the Northern Apennines with a stable isotope analysis to characterize the fluid regime that existed during deformation along this fossil megathrust. Here a 500 m thick fossil fault zone represents the exhumed early Eocene-middle Miocene plate boundary between the European and the Adriatic plates. Along this plate boundary basal and frontal tectonic erosion occurred simultaneously. Both mechanisms were able to incorporate unlithified, fluid-rich sediments into the subduction channel (sensu *Cloos and Shreve* [1988]) (Figure 1a).

2. Tectonic Setting of the Erosive Subduction Channel in the Northern Apennines

[7] The fossil erosive subduction channel was active at least from the early Miocene (~25 Ma) to the middle Miocene (~15 Ma). This erosive subduction zone was preserved because of later deactivation of the plate boundary, followed by its exhumation and partial erosion.

[8] During the Late Cretaceous the convergence and oceanic subduction of the Adria/Africa plate under the European plate [*Coward and Dietrich*, 1989] led to the buildup of an accretionary prism at the front of the European plate [*Treves*, 1984]. Today, the preserved fossil accretionary prism occupies the topmost part of the Apennine tectonic pile. Its frontal, eastern part is formed by offscraped and frontally accreted mud-rich sediments and turbiditic sandstones and limestones [*Vannucchi and Bettelli*, 2002; *Bettelli and Vannucchi*, 2003] of Early Cretaceous to early middle Eocene age. Beginning in the middle-late Eocene (~35 Ma), the lower-slope sediments were deposited on gravitationally disaggregated material of the accretionary prism, which then started to be reworked and was no longer built by frontal accretion.

[9] Two independent events, the occurrence of synkinematic metamorphism at 27 Ma [*Kligfield et al.*, 1986] and the activation of the foredeep [*Ricci Lucchi*, 1986], are the first indications of a change in the Apennine collisional regime during the late Oligocene (~28 Ma) [*Reutter et al.*, 1980; *Malinverno and Ryan*, 1986]. Some authors infer that continental crustal subduction could have started well before the late Oligocene, because the incoming continental margin of the Adria plate is envisioned as a thin crust extending over a width of several tens of kilometers [*Marroni et al.*, 1998]. For this reason it is possible that some of the "oceanic" sediments incorporated in the accretionary prism were in fact deposited on an anomalously thin submarine continental crust. In this case the first stages of continental subduction would not have been significantly different from typical oceanic subduction.

[10] Collision concentrated the deformation on several NW–SE-trending thrust zones that shortened the subducting continental crust, while the no-longer-active accretionary prism remained as an intact forearc on top [*Pialli et al.*, 1998]. This strain concentration occurred progressively from west to east following lithospheric flexure, as indicated, for example, by progressive activation of the foredeep turbidite domains during the Oligocene-Miocene deformation of the western Adriatic margin [*Cibin et al.*, 2001]. Subduction trench migration, compression, and simultaneous formation of extensional basins in the western Mediterranean (e.g., the Liguro-Provençal and Tyrrhenian basins) have led to tectonic models of subduction rollback [*Malinverno and Ryan*, 1986; *Jolivet and Faccenna*, 2000].

[11] The Apennine subduction channel is about 500 m thick. It is formally known among Apennine geologists as the Sestola-Vidiciatico Unit (SVU) (Figure 1). The SVU is presently sandwiched between the overlying Late Cretaceous-early Eocene accretionary prism, that is, the frontal European plate margin and underlying Adriatic continental units. The subduction channel appears as a mélange formed by tectonically and gravitationally reworked blocks of (1) the prior Late Cretaceous-early Eocene accretionary prism, (2) debris flow deposits of the frontal prism, and (3) late Eocene-early Miocene slope sediments originally deposited on top of the frontal prism [*Remitti et al.*, 2007].

[12] Thus the SVU represents a large shear zone between the overriding European plate and the underlying Adriatic plate. It contains material that was both lithified and unlithified at the time of incorporation, and that came from the overriding plate. All of these features are consistent with its being the shallow portion of an erosive subduction channel.

3. The Subduction Channel Components and Their Deformation Prior to Underthrusting

[13] The subduction channel is bounded by a roof and a basal décollement [*Vannucchi et al.*, 2008]. Considering the extension of the fossil accretionary prism on top of the foredeep turbidites, the basal décollement must have accommodated a minimum of 100 km of displacement. The roof décollement at the contact with the overlying fossil accretionary prism has a planar geometry at a regional scale. In contrast, the basal décollement is composed of ramps and flats

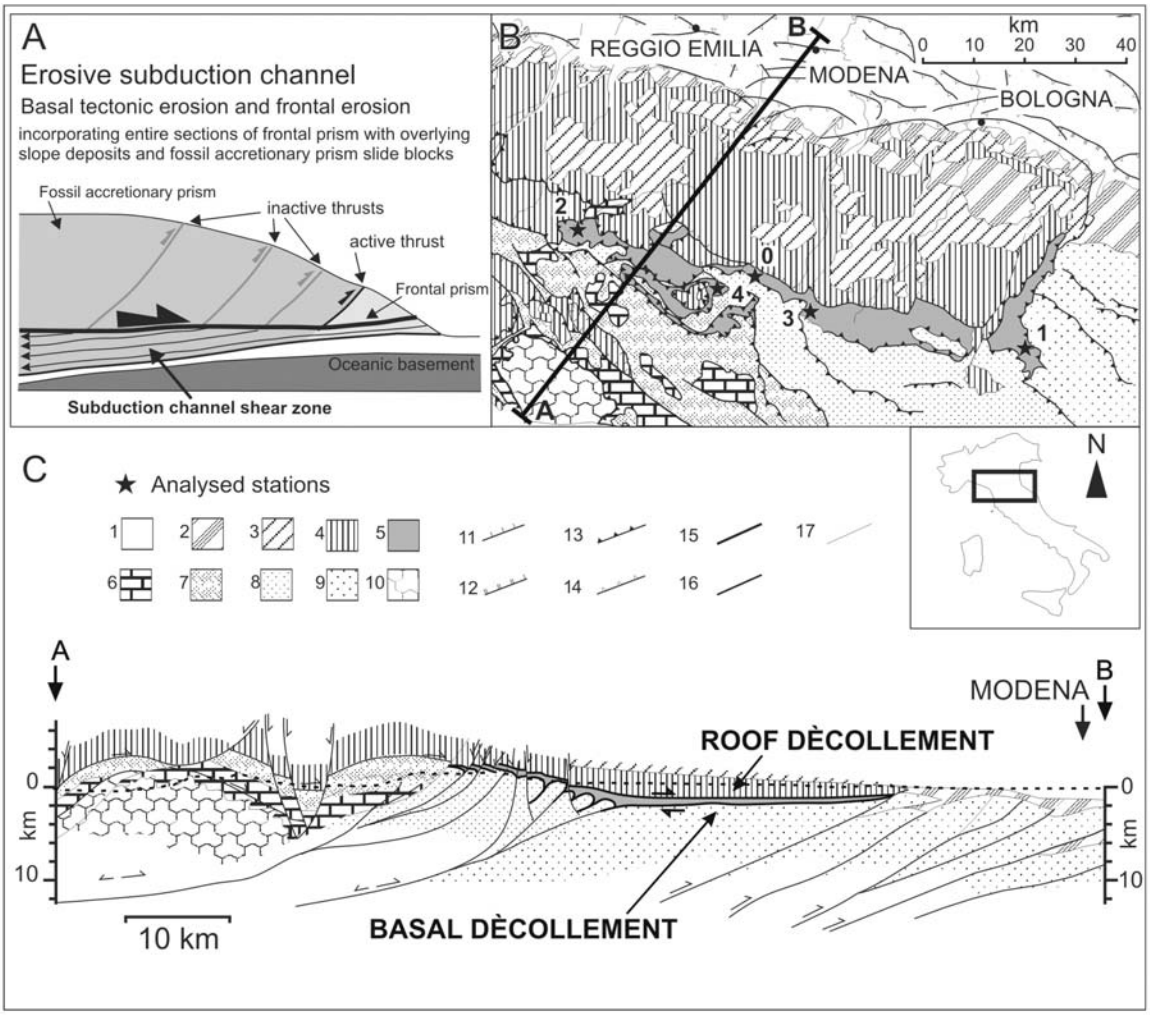

Figure 1. (a) Scheme showing an erosive subduction channel based on reconstructions from the Northern Apennines (not to scale). (b) Schematic geological map of the Northern Apennines, with its geographic location shown in the inset. In this map the location of the sampled outcrops is marked by a star: (0) Montecreto; (1) Firenzuola; (2) Caprile; (3) Vidiciatico; (4) Riolunato. Key to geology: (1) Quaternary deposits; (2) late Miocene-Pleistocene marine deposits; (3) Forearc slope deposits; (4) oceanic units of the Late Cretaceous-early Eocene accretionary prism—European plate; (5) Sestola-Vidiciatico tectonic unit—subduction channel; (6) Mesozoic carbonate units of the Adria plate; (7) late Oligocene-early Miocene (Aquitanian) trench turbitites of the Adria plate; (8) early Miocene (Aquitalian-Burdigalian) foredeep turbidites of the Adria plate; (9) middle Miocene-late Miocene (Langhian-Messinian) foredeep turbidites of the Adria plate; (10) metamorphic continental units of the Adria plate; (11) normal faults; (12) normal faults (subsurface); (13) thrust faults and overthrusts; (14) thrust faults (subsurface); (15) strike-slip faults; (16) high-angle faults of unknown displacement (subsurface); (17) lithological boundaries. (c) Geological cross section of the Northern Apennines as marked in the maps in Figures 1a and 1b. The thickness of the Sestola-Vidiciatico Unit (SVU) is about 500 m and decreases slightly toward the NE.

at the map scale, with the inner outcropping portion (>5 km of overlying sediments) involved in a series of map-scale thrusts and folds with the underlying foredeep sediments.

[14] The present state of strain of the subduction channel is the result of both the deformation history of the different components and the progressive deformation of the complex and chaotic rock mass. Blocks coming from the Late Cretaceous-early Eocene accretionary prism have a deformation history associated with oceanic subduction and building of an accretionary prism, while the blocks of late Eocene-early Miocene slope sediments were not involved in the oceanic tectonic phase and record only subduction channel deformation. The blocks incorporated in the subduction channel responded to deformation according to their different stages of lithification. Once the material entered the subduction channel, it was progressively transported toward

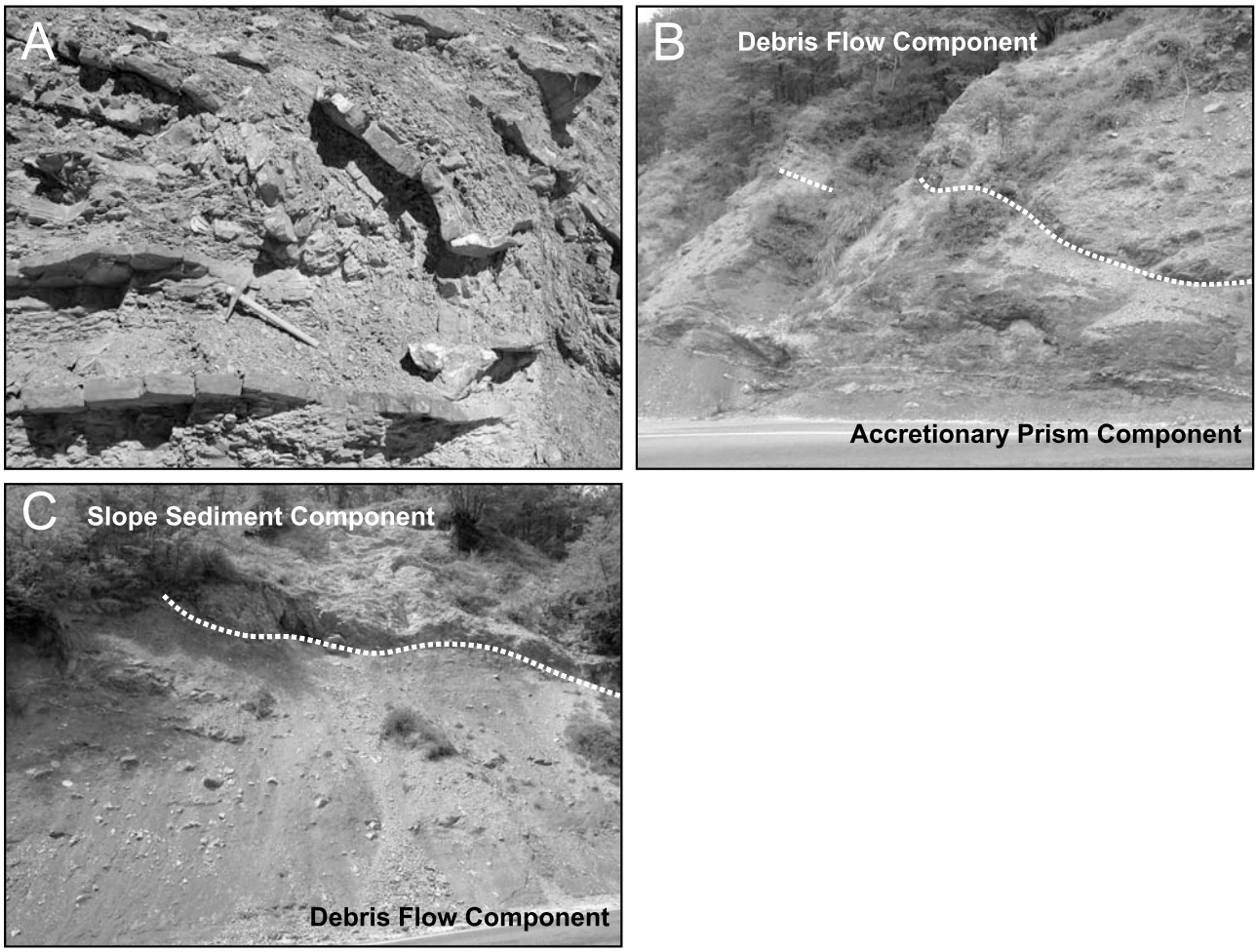

Figure 2. Geological components of the Apennine subduction channel. (a) Block of oceanic sediment involved and deformed in the Late Cretaceous-early Eocene accretionary prism. The photograph shows a fold with boudinaged limbs. (b) Block of debris flow in contact with a block of accretionary prism material. (c) Block of slope sediment in contact with a block of debris flow.

the deeper portions and deformed at increasing pressure and temperature conditions.

3.1. Accretionary Prism Component

[15] Most of the units involved in the frontal part of the Late Cretaceous-early Eocene accretionary prism are now cropping out as a broken formation with a typical block-in-matrix fabric (Figure 2a) [*Vannucchi and Bettelli*, 2002; *Bettelli and Vannucchi*, 2003]. The block-in-matrix fabric is the result of the superposition of two generations of folds deforming a sedimentary multilayer, that is, shales, limestones, and sandstones, which is characterized by a strong contrast in mechanical behavior [*Vannucchi and Bettelli*, 2002; *Bettelli and Vannucchi*, 2003]. Folding produced a complete transposition of the original bedding and the shale interbeds are characterized by a strong scaly fabric. The polyphase deformation generating the block-in-matrix fabric was also associated with vein development [*Bettelli and Vannucchi*, 2003]. In the channel this component is present as blocks of various sizes, ranging from single boudin or vein fragments, mainly in the debris flow, to large portions where the original block-in-matrix fabric is preserved. For the purpose of the present paper both the sediments and the veins associated with the accretionary prism represent potential source rocks for the fluids that circulated within the subduction channel.

3.2. Debris Flow Component

[16] The debris flow component is represented by polymictic sedimentary breccias formed by reworking of the frontal part of the accretionary prism and the overlying slope sediments. Limestone, sandstone, and shaley clasts of variable sizes are randomly dispersed within a pelitic matrix [*Bettelli and Panini*, 1989; *Bettelli et al.*, 1996; *Pini*, 1999; *Vannucchi et al.*, 2003] (Figure 2b). Distinction between clasts and matrix can be done only using an arbitrary grain size criterion [*Swarbrick and Naylor*, 1980; *Abbate et al.*, 1981]. Locally, these breccias also contain large blocks in which the original stratigraphy of the source rock is still preserved. Commonly, at the outcrop scale, a penetrative network of anastomosing surfaces defines a prominent scaly fabric cleavage that is generally parallel to the stratigraphic layers (Figure 2b). We think that this geometry is caused by dewatering and the subsequent pore

collapse associated with compaction [*Vannucchi et al.*, 2003]. Locally, the scaly fabric cleavage is cut at a very high angle by a later net of closely spaced shear surfaces (Figure 2b). These shear surfaces, commonly coated with very thin calcite veins, are generally parallel to the boundaries of the blocks of the former accretionary prism involved in the debris flow. Further evidence of deformation accompanying compaction within the debris flows is the presence of asymmetrical shadows around the harder clasts; however, these structures and their relationships are difficult to interpret. For example, shear sense indicators do not provide unequivocal and reliable results. Both the scaly fabric cleavage and the shear surfaces are cut by a network of mesoscopic brittle faults (Figure 2b) containing calcite veins that crosscut all components of the mélange.

3.3. Slope Sediment Component

[17] The late Eocene-early Miocene slope sediments are incorporated in the subduction channel as coherent blocks that can be up to 10 km wide and 100 m thick (Figure 2c). They are formed by late Eocene-early Oligocene dark gray or reddish silty mudstones (Fiumalbo shales) and thick late Oligocene-early Miocene (Aquitanian) packages of marls (Marmoreto marls). Thin- and thick-bedded turbidites of different grain composition are also present (Vallorsara sandstones, Sassolera member). Originally, the slope sediments were unconformably deposited on the frontal part of the former accretionary prism, locally reworked by mass wasting processes, and intermixed with debris flows and mudflows. Slumps, folds, pinch-and-swell structures, and symmetric boudins are also present, embedded within packages of unfolded strata.

[18] The contacts between the different portions of the late Eocene to Miocene slope sediments were stratigraphic at the time of their deposition. Their early deformation can be linked to the instability of the frontal prism. Locally, the shaley and the marly formations were thickened by repetition that was seldom accompanied by evidence of thrusting in these yet-to-be-lithified sediments [*Remitti*, 2005]. The early deformation suggests that the late Eocene to early Oligocene sedimentation took place on a tectonically active slope where the unstable environment commonly caused slope failures, with development of repetitions and slumps.

[19] At present, the original thrust contacts have been completely destroyed. The kinematic indicators along the contacts between repeated units commonly represent normal or strike-slip faults. Furthermore, these faults now display different superimposed slickenlines, and in general, the faults are coated by calcite veins. We conclude that this is a consequence of their incorporation into the subduction channel.

[20] These late Eocene-early Miocene lower-slope deposits were incorporated in the subduction channel during contemporaneous overthrusting of the former accretionary prism and underthrusting of the foredeep deposits. The subduction channel activity is regionally shown by incorporation of (1) Aquitanian to Langhian, and perhaps early Serravallian, slope or basin-margin deposits (Monte San Michele marls, Baigno marls/Suviana sandstones); (2) Aquitanian to Burdigalian slices of the basal sediment of the Burdigalian foredeep deposits (Civago marls, Serpiano sandstones); and (3) Aquitanian to Burdigalian and Langhian to Serravallian inner-slope portions of the most recent foredeep sequences [*Bettelli and Panini*, 1992; *Landuzzi*, 1994; *Bettelli*, 2002; *Bettelli and Boccaletti*, 2002].

4. Strain Evolution Inside the Subduction Channel With Associated Vein Development

[21] The slope sediment is the only component that did not enter the subduction channel as a preexisting mélange. For this reason it represents the ideal unit with which to study the deformation history within the erosive subduction channel. The slope sediments became involved in the subduction channel when they had yet to be completely lithified. The occurrence of fractures, faults, and veins, versus flow structures, such as flames, and hydroplastic fractures, as well as pinch-and-swell structures, indicates that the marls were the first to reach complete lithification, while coeval sandstones and shales were still able to deform as soft sediments. When sandstone layers were finally cemented and deforming rigidly, shales were still able to flow. These compaction and lithification processes provided a large volume of released fluids that strongly influenced the deformational response of the subduction channel.

[22] The variable stages of progressive lithification of the sediments made the deformational response to applied stresses very different for the different components. Each type of sediment is characterized by its own structural progression, which led to a diachronous evolution of deformation within the channel. In the field we observe the concentration of the deformation within the weakest inclusions and along the contacts between various sediment types

Figure 3. Photograph showing the deformation features in the shallow portion of the subduction channel. (a) Pervasive normal faults cutting through marls of the slope sediment at the meter to centimeter scale, with the flattened bipyramid (arrows) showing the three-dimensional shape of sediment elements cut by the pervasive normal faults. (b) Equal-angle, lower-hemisphere stereographic projections of pervasive normal faults and associated striae and rose diagrams of the striae in Montecreto and Riolunato. (c) Hydroplastic fractures (some of them marked with a white arrow) in sandstone layers forming a chocolate-tablet boudinage. (d) Thin section of a deformation band along a hydroplastic fault (displacement, ~1 cm). The band boundary, going from the top left to the bottom right, separates the wall rock, at the bottom, from the band, to the top. The amount of calcite cement, brownish red in the photograph, increases sharply across the boundary, which indicates positive dilatancy. The dark color suggests a preferential circulation of fluids along the band. Mica grains (white arrows) are bent at the boundary of the deformation band. Inside the band the quartz grains have maintained their original size, while the mica grains have been crushed. (e) Stretched crystals of calcite and barite inside an extensional vein in sandstone. (f) Crack-and-seal extensional calcite and quartz vein parallel to the terminations of a sandstone boudin. In the photograph the crack and seal is particularly evident in the stretched crystals of quartz characterized by trails of fluid and solid inclusions (indicated by the white arrows) that parallel the vein border.

through the development of detachment surfaces. The localization of deformation within less lithified sediments implies that the shales most likely affected the bulk permeability of these units since they provided a very good seal that probably contributed to the development and preservation of high fluid pressures for long periods of time within the mélange.

[23] Selected outcrops were chosen for both microscope observations and stable isotope analyses. These outcrops (Figure 1a) were also studied with detailed structural analyses. The deformation of the sediment incorporated in the subduction channel is linked to the total underthrusting experienced by these sediments, that is, the distance they reached from the deformation front, and to the progressive increase in the overburden represented by the former accretionary prism and slope sediments. The strain evolution in the subduction channel is described according to three main structural associations that define the prevailing tec-

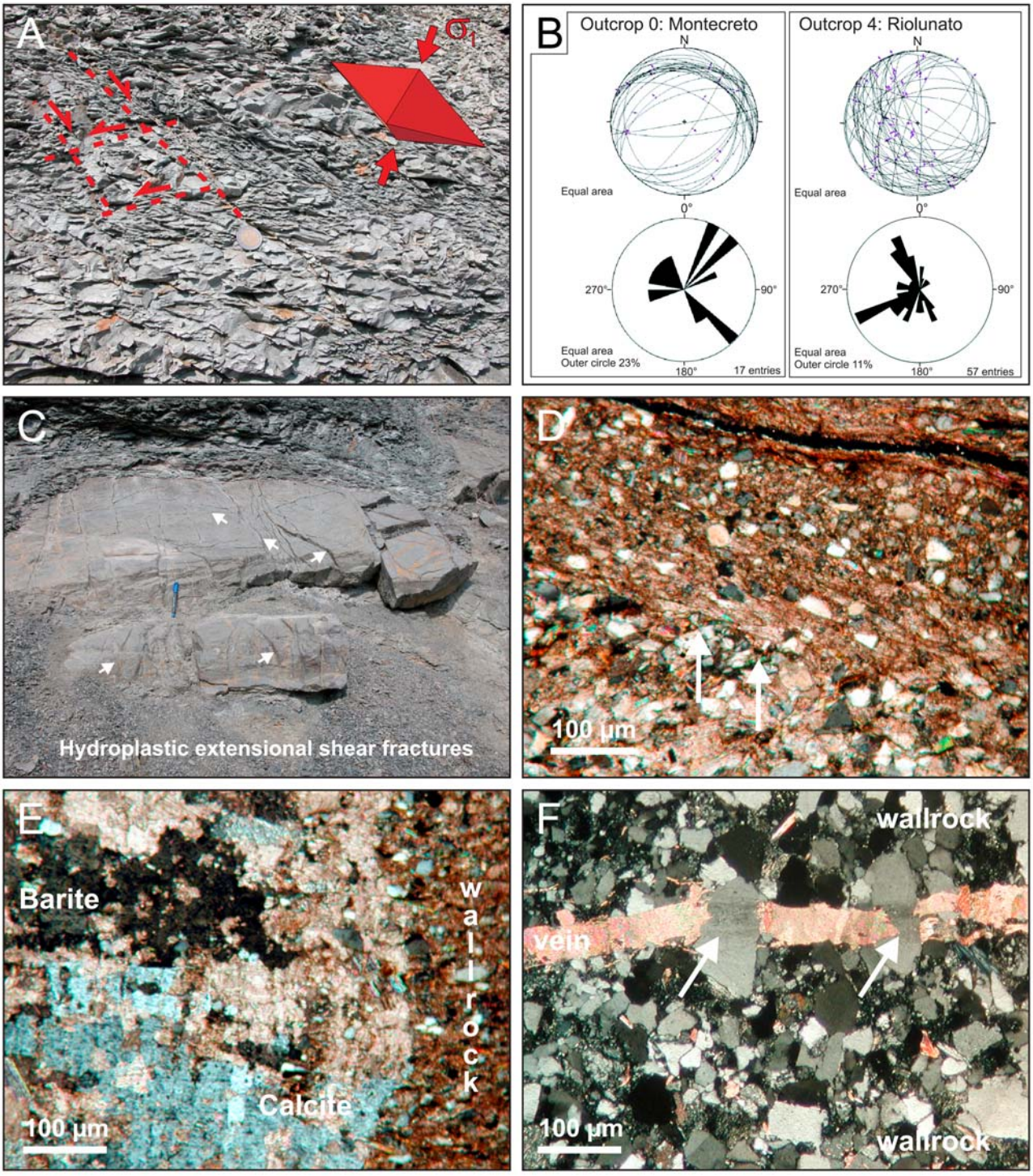

Figure 3

tonic regimes: a shallow zone, an intermediate zone, and a deep zone. The chosen outcrops expose portions of the subduction channel and/or their typical deformation style at increasing paleodepth. Outcrop 0, Montecreto, shows a good record of the shallowest deformation features, characterized by no mineral precipitation (Figures 3a and 3b). Outcrop 1, Firenzuola, and outcrop 2, Caprile, represent the intermediate part of the subduction channel, and the remaining two, Vidiciatico and Riolunato, represent the deepest exposed part.

[24] The structural associations have been correlated with a corresponding depth determined from the thickness of overlying sediments or, when possible, on P and T indicators. The orientation of the state of stress within the subduction channel has been inferred based on the dynamics of deformation structures, consisting mainly of faults, shear zones, and veins. Possible variability of dynamically and kinematically induced stress conditions along the subduction channel did not influence the three-dimensional (3D) architecture of the deformation structures, which reveal consistent structural patterns at the outcrop scale.

4.1. The Shallow Zone ($\lesssim$3 km Depth): Pervasive Extension

[25] The first and oldest deformation recorded in the late Eocene–Miocene blocks is pervasive deformation that leads, in some cases, to complete obliteration of the bedding. While the shales generally show scaly fabric, the marly sediments are pervasively cut by sets of scale-invariant shear surfaces down to the millimeter scale (Figure 3a). Slickensides collected on the shear surfaces show normal movement; only a few measurements imply reverse faulting. The field data sets (Figure 3b) consistently show two contemporaneous systems of gently dipping normal faults, each formed by two conjugate sets. The resulting 3D geometry is comparable to that of a flattened bipyramid (Figure 3a). The planes of symmetry of the flattened bipyramid are parallel to the bedding when the lateral continuity of the beds is preserved. Hence, the two directions of extension are normal and parallel to the main direction of tectonic transport.

[26] The bipyramids have their minor axis nearly parallel to the vertical direction where the faces show angles of 110°–120°; that is, the two observed conjugate shear planes are inclined at an angle of >45° to the axis of maximum compressive stress, σ_1 (Figure 3a). Although a high angle is consistent with unconsolidated, hence very weak, sediments, brittle failure criteria cannot fully explain the observations. Apparently, this shallower portion of the subduction channel accommodated strain through contemporaneous failure and compaction, the latter inducing flattening of the bipyramids but not enough compaction to induce pressure solution or deform the sediment grains. The faults tend to die out along the contact with the already lithified pieces of the mélange, indicating strong differences in mechanical behavior between its components.

[27] These pervasive conjugate normal faults in the marls do not contain veins (Figure 3a). However, they are commonly coated with a thin Fe-oxide film. The later veins cut and/or show zones of oxide inclusion within calcite, suggesting syntectonic precipitation of the oxides and fluid circulation along the fracture.

[28] Pervasive conjugate normal faults in the marls formed contemporaneously with the development of hydroplastic fractures/faults [*Petit and Laville*, 1987; *Bettelli and Vannucchi*, 2003; *Remitti*, 2005] in the sandstone layers (Figure 3c). They are characterized by the principal surface of fracture gradually disappearing above and below, with the texture of the rock changing parallel to the bedding plane to become a mere granulation of the fracture surface. These fractures typically formed in unlithified sediments. The hydroplastic fractures have the same geometry as the pervasive normal faults and produce boudinage in two roughly perpendicular directions, resulting in a chocolate tablet structure [*Ramsay and Huber*, 1983] (Figure 3c).

[29] In thin section each hydroplastic fracture is sealed so that no discontinuity is visible in the grains or in their organization. The hydroplastic fractures display a small positive dilatancy indicated by a relative increase in calcite cement (Figure 3d). The calcite cement has a reddish-brown color and locally it contains a few sparse grains of sandstone corresponding to the fracture termination. These characteristics suggest preferential fluid circulation within these fractures and oxide deposition in a chemical environment different from the surroundings (Figure 3d). Compaction and lithification processes provided a large volume of released fluids that strongly influenced the deformational response of the subduction channel.

[30] From the foregoing observations it appears that a large fraction of the sediments was still unlithified when they were incorporated in the subduction channel, which provided a large volume of fluid release. In the shallowest zone of the subduction channel the contemporaneous presence of failure and compaction and the development of hydroplastic fractures is evidence of considerable fluid circulation, but without the development of veins.

[31] The oldest extensional veins occur at the edges of sandstone boudins that cut preexisting hydroplastic fractures. These veins are calcite or mixed calcite-barite and calcite-quartz (Figures 3e and 3f). In all cases the crystals are fibrous, straight, parallel to the bedding, and perpendicular to boudin terminations. Most of these veins can be classified as stretched-crystal fiber veins with a crack-and-seal texture [*Ramsay*, 1980; *Ramsay and Huber*, 1983] (Figure 3f). The rest are antitaxial veins.

[32] Veins containing calcite and barite crystals are commonly centimeters thick. They display very irregular boundaries as they follow the contacts between different detrital quartz grains (Figure 3e). Mixed calcite-quartz veins are submillimeter thick, show straight contacts with the wall rock, and cut through the quartz grains (Figure 3f). Vein growth is clearly ataxial and the calcite crystals have both weak fibrous shapes and weak crack-and-seal textures.

[33] Quartz-calcite veins develop within sandstones characterized by highly interlocked quartz grains that show evidence of pressure solution at their contacts. These veins are found in sandstones without calcite cement, implying that the circulating fluid did not derive directly from the neighboring wall rock. Instead, calcite-barite veins are developed in siltstones composed of a great variety of detrital grains with a carbonate cementation.

[34] The veins are strongly controlled by the sandstones, while shales are still flowing in pinch-and-swell structures

or in between boudins, implying a difference in the response to the applied stresses between the sandstones and the shales. We think this is best explained if the shales were still unlithified when boudinage occurred, while the sands were at least partially cemented.

[35] From the preceding observations it appears that the sandstones and the shales had different lithification in response to deformation, burial, and increasing dewatering. While sandstones began to deform in a brittle fashion, shales were still able to deform by continuum flow processes.

4.2. The Intermediate Zone (From ~3 to ~5 km Depth): Localized Extension

[36] In this zone diffuse deformation evolves from pervasive faulting to a network of shear zones where the strain is concentrated within bands 10 cm to 1 m thick (Figure 4a). Within the shear zones shear also is not uniformly distributed but, instead, is concentrated along slip surfaces. Shear zones tend to be parallel to the basal and roof décollement except when they reuse preexisting discontinuities (Figure 4). Rarely, there is the development of a fault gouge, while commonly, slip is partitioned into a dense and anastomosing array of extensional veins subparallel to the shear zone itself. These veins also display dilational jogs that increase in frequency toward the deeper portion of the outcropping subduction channel (Figure 4). The dilatant character of the veins implies that fluid pressure was often, at least locally, greater than the least principal stress.

[37] The shear zones are further cut by mesoscopic, discrete faults characterized by a good lateral continuity (lengths of 20–30 m are common) and filled with calcite veins about 1 cm thick (Figure 4c). Less frequently, the shear zones cut and displace these faults. Both the shear zones and the faults have a spacing of tens of meters. Faults have unsystematic orientations, being either steep or horizontal as they reuse preexisting discontinuities as lithological contacts or shear surfaces. Kinematic analysis of these faults provided reliable data from well-preserved slip indicators. Most faults are normal or strike-slip faults, while thrust faults are extremely rare. Normal fault movements cluster toward the NE, NW, SE, and SW. The fault data indicate that the subduction channel has been stretched in two perpendicular directions: (1) a SW–NE direction parallel to the main direction of the Apennine tectonic transport and (2) a perpendicular NW–SE direction.

[38] The discrete normal faults not only cut the shear zones parallel to the basal and roof décollement, but also cut the well-exposed basal décollement (Figure 4d). These crosscutting relationships indicate that in the intermediate zone of the subduction channel, the basal décollement becomes locked and slip migrates upward to other, parallel, shear surfaces. Eventually, these shear surfaces also sealed, yet the roof décollement is not cut by normal faults. The subduction channel's total displacement was thus partitioned between the different shear zones.

[39] Each normal fault accommodates a total displacement varying from ~1 to ~15 cm. The displacement resulted from a great number of smaller movements as indicated by incremental growth of the calcite veins. The shear zones and faults cut all the components of the mélange, but they are best developed inside the marls and the shales. The various components of the subduction channel responded equally to the applied stress, implying that by this stage they had reached a relatively uniform bulk lithification.

[40] The internal structure of the veins is characterized by mutually crosscutting, incrementally developed shear portions and extensional portions. The extensional portions have dark, subhorizontal surfaces connecting the vein walls (Figures 5a and 5b). Commonly, the veins break along these surfaces. The surfaces have slickenfibers showing directions different from the others. The opening direction of the extensional veins parallels the slickenfibers of the associated surface. The two structures therefore had the same growth direction and they are inferred to have formed simultaneously. In thin section these surfaces give the veins a striped appearance: straight and parallel to each other in thin sections oriented parallel to the movement of the fault, and anastomosing in thin sections oriented perpendicular to fault displacement (Figure 5). These surfaces can be characterized either by trapped and sheared minerals and fragments of the wall rock or by a concentration of insoluble material, suggesting that pressure solution was active soon after vein precipitation (Figure 5c). They are similar to the "inclusion trails" described by *Koehn and Passchier* [2000].

[41] Each vein stripe is, in turn, the result of the crystallization either of a great number of sigmoidal-shaped cavities or of a single crack. In the first case the stripe is formed by sets of extensional veinlets separated by solid inclusion bands oriented from 80° to 50°–60° from the shear surfaces (Figures 5a and 5b). The result is a crack-and-seal texture where each extensional veinlet represents an incremental growth of the main vein and where the shear surfaces were active at 50°–80° to σ_1 (Figure 4e). Calcite crystals pass without optical changes across solid inclusion trails (Figure 5b) displaying an elongate/blocky shape and, also, commonly display mechanical twinning.

[42] Along the same vein stripe, the crack-and-seal texture alternates with portions characterized by blocky calcite crystals. In this case the texture, clasts floating in a blocky calcite cement, corresponds to a breccia (Figures 5e and 5f). The clasts are fragments of wall rock, preexisting veins, and preexisting crystals. Calcite clasts are broken by sharp fractures, with the fragments clearly separated by the crystallization of new material (Figure 5f). The calcite clasts are neither rotated nor sheared. The breccia is bounded by shear surfaces not involved in the brecciation itself. The breccia is never cut by the crack-and-seal texture, which implies that when brecciation developed the mechanics of deformation inside the veins changed drastically.

[43] In summary, each vein is formed by several overlapping stripes resulting from a combination of shear elements, that is, the dark surfaces, and extensional elements, namely, the calcite-filled cracks. Inside each stripe, calcite is characterized by different textures, that is, crack-seal or breccias, indicating different opening processes. The characteristics of the pressure-solution seams are consistent both with a cavity collapse between two successive extensional openings and with shearing along the surfaces. Striped veins are cut by submillimeter-thick extensional veins (Figure 5d). Usually the later set of extensional veins is oriented at a high angle to the fault walls (Figure 5d).

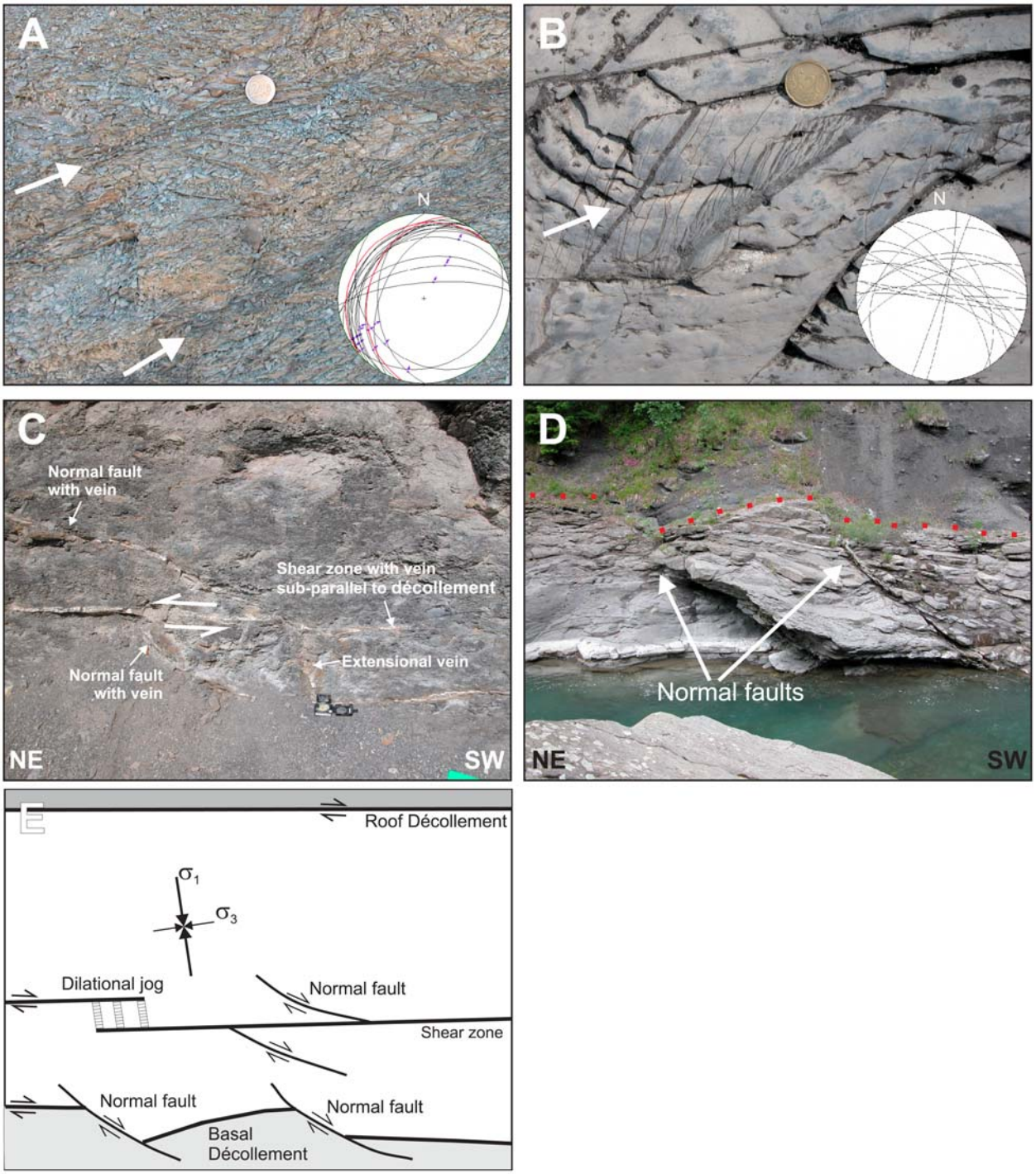

Figure 4. Photograph showing the mesoscopic deformation features in the intermediate portion of the subduction channel. (a) Shear zones (white arrows) subparallel to the basal and roof décollements. Inset: stereoplot (equal area, lower hemisphere) of shear zones (18 data points; arrows show the hanging-wall movement) compared to principal décollements (in red) from near outcrop 3. The shear zones have a general NE vergence. (b) Dilational jog in marls of the slope sediments with extensional veins inside the jog. Inset: stereoplot (equal area, lower hemisphere) of extensional veins inside jogs cutting through a shear zone; 14 data points. (c) Shear zone, with calcite vein, subparallel to subduction channel boundaries, and normal fault, with calcite vein mutually displaced. A subvertical extensional vein is also present. (d) Basal décollement (dotted red line) separating the SVU/subduction channel, debris flow component, from the underlying foredeep turbidites of the Adria plate. The basal décollement is cut by high-angle normal faults (white arrows) filled by calcite veins that have displacements of about 1–2 m toward the SW. (e) Sketch, not to scale, of the geometrical relationships among shear zones, normal faults, and extensional veins in the Apennine subduction channel and the inferred state of stress.

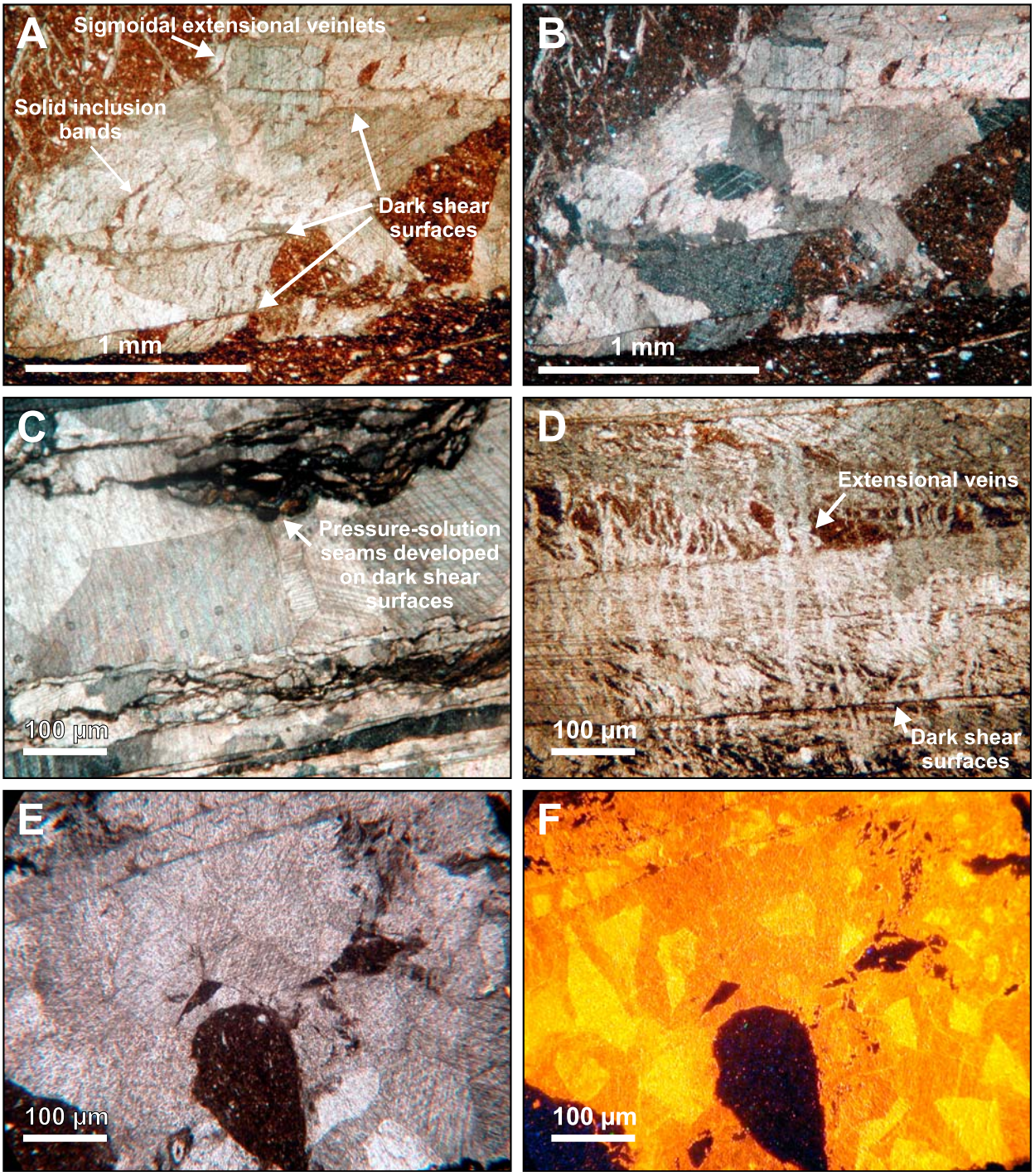

Figure 5. Photograph showing the microscopic deformation of structures developed in the intermediate portion of the subduction channel. (a) Thin section, in plain polarized light, showing a crack-and-seal portion of a striped vein cut parallel to the movement of the fault. Typical elements (extensional sigmoidal veinlets, dark sear surfaces, and solid inclusion tracks) are shown. Displacement is anticlockwise and parallel to the lower edge of the picture. (b) Same as Figure 5a, but in crossed polars showing the elongated calcite crystals that are nontracking the opening direction of the vein. (c) Striped vein cut perpendicular to the vein lineation. The dark shear surfaces are wavy and branching. Pressure solution features developed in correspondence with dark surfaces after veinlet precipitation. Crossed polars. (d) Extensional veins cutting through a pre-existing calcite-striped vein. The set of extensional veins is oriented at a high angle to the dark surfaces, which are usually parallel to the vein walls, as in this case. Plane polarized light. (e) Thin section, plane polarized light, of a brecciated sector of a striped vein. (f) Same thin section as in Figure 5e but in cathodoluminescence, showing brecciated wall rock and pre-existing calcite crystals wrapped by a younger phase of calcite mineralization.

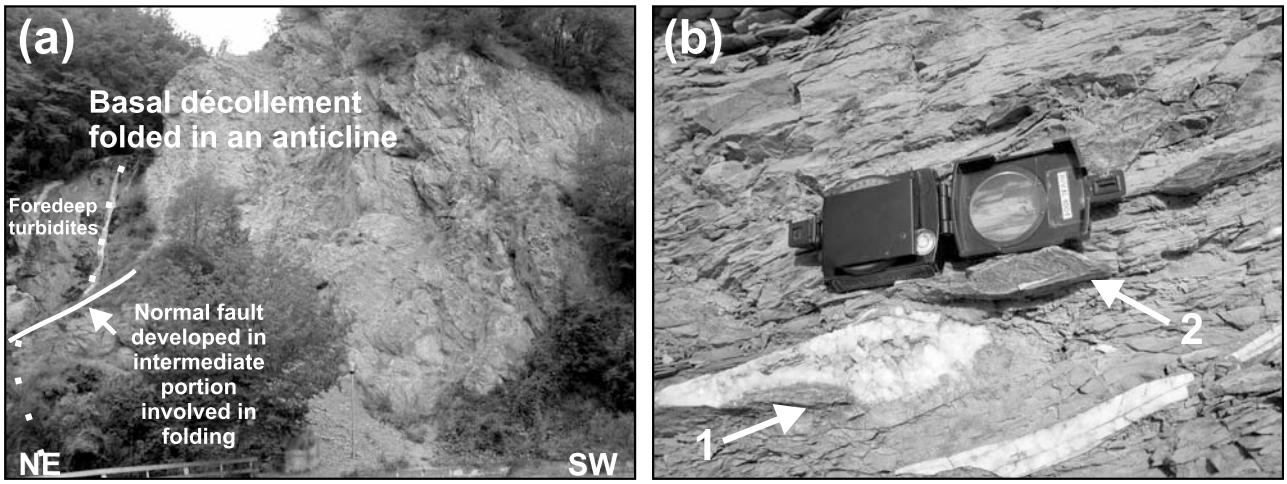

Figure 6. (a) Photograph showing the basal decollément in the deep portion of the subduction channel. Here the basal decollément is involved in an anticline fold, indicating shortening. Veins (black arrow) are also associated with this phase of deformation. (b) Dilational jogs: (1) filled by blocky calcite; (2) formed by extensional veins oriented at a high angle to the shear zone.

4.3. The Deep Zone (≳5 km Depth): Contraction

[44] In this portion of the subduction channel, clay mineral assemblages, fluid inclusions, reflectance of organic matter [*Reutter et al.*, 1992], and fission tracks [*Zattin et al.*, 2000] indicate that the sediment reached ~120°–150°C [*Reutter et al.*, 1992; *Zattin et al.*, 2000], which typically corresponds to a depth of ~5 km. In modern subduction zones, 150°C is usually thought to be a key threshold temperature marking the updip limit of seismogenesis [*Moore and Saffer*, 2001].

[45] The deepest outcropping zone of the subduction channel is involved in large-scale (i.e., tens to hundreds of meters) fold-and-thrust deformation involving both the basal décollement and the lower part of the subduction channel (Figure 6a). Foredeep deposits, which show neither extension nor contraction in shallower portions, are also involved in these deeper fold-and-thrusts. The deactivation of the basal décollement, already inferred from its intersection with normal faults intersection in the intermediate zone, is also indicated here. The different involvement of the two boundaries in the fold-and-thrust development indicates that while the roof décollement was still active and responsible for the northeastward migration of the upper plate on top of the foredeep turbitites, the basal décollement was already deactivated. There are no mesoscale contractional structures.

[46] The frequency of veins increases in comparison to that in the previous intermediate zone, suggesting that fluids were still present. Here, too, dilational jogs start to be common along the principal shear surfaces that parallel the main décollements (Figure 6b). The stepover region shows finite increments of dilatation associated with slip transfer across the jog. The stepover width of these dilational jogs approaches ~10 cm. Vein textures record histories of incremental growth, with shearing increments along the main décollement/shear zone accompanied by significant dilatation in the stepovers.

[47] The calcite infilling of the jog records the associated influx of fluids. Shearing across the stepover region is accommodated by mesh structures with principal components that include either a set of subvertical millimeters- to centimeters-thick extensional veins or brecciation (Figure 6b). The extensional veins have an internal fabric similar to that of the crack-and-seal veins (Figure 6b). Orientations of the various components are broadly compatible with the inferred NE–SW regional stress field.

[48] Part of the contractional deformation in the outcropping deepest zone of the subduction channel can be associated with concentrated collisional shortening. Nevertheless, the subduction channel was still active as demonstrated by the ongoing underthrusting of undeformed foredeep turbidites at the front of the system.

5. Stable Isotope Compositions of Calcite Veins

5.1. Sampling Methods and Analytical Techniques

[49] C and O isotope compositions of 125 calcite vein and 83 host rock samples were analyzed from four outcrops within the 500 m thick subduction channel (Figure 1). Each outcrop is characterized by particularly fresh material that can extend for ~1000 m^2. Colocated sampling was done for stable isotope analyses and structural observations.

[50] Sampled rocks and selected veins were mechanically drilled from polished surfaces. Each powdered sample was then reacted with orthophosphoric acid at 25°C under vacuum for 12 h [*McCrea*, 1950]. The isotopic compositions ($^{13/12}$C and $^{18/16}$O ratios) of the resulting CO_2 were measured at the IGG-CNR (Institute of Geosciences and Earth Resources National-Research Council of Italy, Pisa) using Thermo-Finnigan Delta XP isotope ratio mass spectrometry. Results are reported according to the conventional δ-notation Vienna Peedee belemnite (PDB) and Vienna SMOW. Proper standardization for the O and C isotope analyses was verified by international carbonate standards, including NBS-19 (calcite), and an internal calcite standard.

The internal standard (Carrara marble), used in IGG-CNR stable isotope laboratories since the 1970s, has an uncertainty (expressed as 1σ) of <0.10‰ for both $\delta^{18}O$ and $\delta^{13}C$. This sample is regularly added to the sample sets (five samples per set) for each run of measurements.

[51] Stable isotope analyses provide an independent measure to potentially identify (1) evidence of fluid-rock interactions in the Apennine plate boundary zone during its evolution, (2) the source of these fluids, and (3) evidence of diffuse versus confined fluid flow. Since stable isotope analysis and structural observation require quite different approaches to data description, only after first presenting the isotopic analyses do we synthesize these observations to define the nature of fluid flow within the subduction channel.

[52] Stable isotope analysis was performed on the host rocks and their associated veins developed during subduction channel activity. The host rocks sampled in the subduction channel are represented by (1) slices coming from the former accretionary prism, (2) slope sediment, and (3) debris flow component. The debris flow component results from reworking of the other two; they were distinguished by the origin of the clasts (Figure 7). All these hanging-wall rocks were analyzed to characterize potential end-member sources of the fluids that produced calcite vein precipitation. An alternative source rock is represented by the Foredeep turbidites located in the footwall.

[53] We considered the veins developed during the former accretionary prism phase together with the prism source rocks. For the vein sampling within the subduction channel we differentiate each vein with respect to its own host rock (Figure 7b) and with respect to the location (Figure 7c), to investigate the different fluid/rock interactions and/or the regional variability. In addition, we singled out those veins marking the basal decollément, that is, located at the boundary between the subduction channel and the foredeep turbidites (Figure 7c). Finally, in the Firenzuola outcrop (Figure 1, no. 1) we sampled veins developed within the foredeep turbidites (Figure 7a). This location is the only one showing veins in the foredeep turbidites close to the subduction channel.

5.2. Results

[54] Results for the oxygen and carbon isotope distributions in the four analyzed outcrops are summarized in Table 1 and Figure 7a. Figures 7b, 7c, and 8 show the $\delta^{13}C$ and $\delta^{18}O$ values for the different components of the subduction channel. Data averages were also calculated (Table 2); these are interpreted as reflecting regional variations.

[55] The $\delta^{18}O$ values for the accretionary prism source rock are negative and quite uniform, being in the range of −4.7‰ ± 2.2‰/−6.5‰ ± 1.7‰ PDB, whereas those for the slope sediments are highly variable, −1.7‰ ± 1.2‰/−6.6‰ ± 0.5‰ PDB. The foredeep turbidites forming the footwall of the subduction channel have average $\delta^{18}O$ values very similar to those of the slope deposits of the same outcrop, −6.8 ± 1.4 ‰ PDB (Figure 8).

[56] The $\delta^{18}O$ values for veins developed within the subduction channel are generally lower than those of the subduction channel components. For the accretionary prism $\Delta^{18}O_{SCV\text{-}APS}$ (subduction channel veins-accretionary prism source rock) varies from −0.3‰ to −2.0‰ PDB; for the slope sediments $\Delta^{18}O_{SCV\text{-}SSS}$ (SCV-slope sediment source rock) varies from −2.2‰ to −5.1‰ PDB; and for the foredeep turbidites $\Delta^{18}O_{SCV\text{-}FTS}$ (SCV-foredeep turbidites source rock) is −2.9‰ PDB (Table 2).

[57] Regional variations in stable isotopic data show that the $\delta^{18}O$ values in the SCVs decrease from −5.9‰ ± 1.7 ‰ to −9.8‰ ± 0.4‰, moving deeper in the channel (Figure 7c and Table 2). At two outcrops, Vidiciatico and Riolunato, it is possible to directly compare the $\delta^{18}O$ values of the veins along the basal décollement with those of the channel. The veins developed at the basal decollément are laterally continuous and mark a specific surface. While Riolunato maintains the same values, Vidiciatico shows more negative values along the basal décollement, −8.7‰ ± 0.8 ‰ PDB, than within the channel, −7.8‰ ± 0.5‰ PDB.

[58] The $\delta^{13}C$ values show less variability at the deepest outcrop. Overall positive $\delta^{13}C$ values characterize the APS rocks, while negative $\delta^{13}C$ values characterize the slope sediment, the SCVs, and the foredeep turbidites (Table 1).

[59] The source rocks, first involved in the accretionary prism and later incorporated into the subduction channel, have an average $\delta^{13}C$ value of 0.5‰ ± 0.6 ‰ PDB. The $\delta^{13}C$ values for the slope sediments vary from −0.5‰ ± 0.9‰ to 0.4‰ ± 0.3‰ PDB ($\delta^{13}C_{average}$ = 0.1 ± 0.8). The Foredeep turbidites forming the footwall of the subduction channel have average $\delta^{13}C$ values of 0.4‰ ± 0.3‰ PDB. The $\delta^{13}C$ data of the Chattian Aquitanian turbidites (~25–22 Ma) are more uniform than those of the Burdigalian turbidites (~20–18 Ma) (Table 1).

[60] The $\delta^{13}C$ values for veins developed within the subduction channel are generally lower than those of the subduction channel components. $\Delta^{13}C_{SCV\text{-}APS}$ varies from −0.8‰ PDB to −3.2‰ PDB. $\Delta^{13}C_{SCV\text{-}SSS}$ varies from −1.4‰ PDB to −0.2‰ PDB. $\Delta^{13}C_{SCV\text{-}SRC}$ is −0.6‰ PDB.

[61] Regional variations in stable isotopic data show that the $\delta^{13}C$ values in the SCVs slightly increase moving deeper in the channel from −2.0 (±0.9) ‰ PDB to −0.2 (±0.7) ‰ PDB (Figure 7c). The comparison between the $\delta^{13}C$ values of the veins within the channel with those along the basal décollement reveals lower values for the latter in both outcrops. It is worth noting that Firenzuola (outcrop 1), is known for the presence of Miocene CH_4-rich fluid veins supporting chemosynthetic communities [*Conti and Fontana*, 2005]. This site differs from the other localities: its carbonate veins have the lowest value of −3.4‰ $\delta^{13}C_{PDB}$ (Figure 8). In this area, the foredeep turbidites of the Adriatic underthrusting plate commonly contain limestones associated with a lucinid clams-dominated macrofauna [*Tavani*, 2001], which are characterized by $\delta^{13}C_{PDB}$ values from −16‰ to −58‰ [*Terzi et al.*, 1994]. These limestones have been interpreted as methanogenetic chemoherms [*Terzi et al.*, 1994]. Their occurrence is not surprising since cold venting is now recognized to be common in many subduction zones [*Sample et al.*, 1993; *Lewis and Marshall*, 1996; *Suess et al.*, 1998; *Sahling et al.*, 2008]. At outcrop 1, the correlation of $\delta^{13}C$ values for veins of the subduction channel with those of the foredeep turbidites (−27.0‰ < $\delta^{13}C_{PDB}$ < −12.3‰) is therefore in line with the nearby situation; this influence is not visible in the other outcrops. This result supports the hypothesis that the shallow and intermediate part of the subduction channel is permeable to pore fluids from the underthrusting plate that interacted with

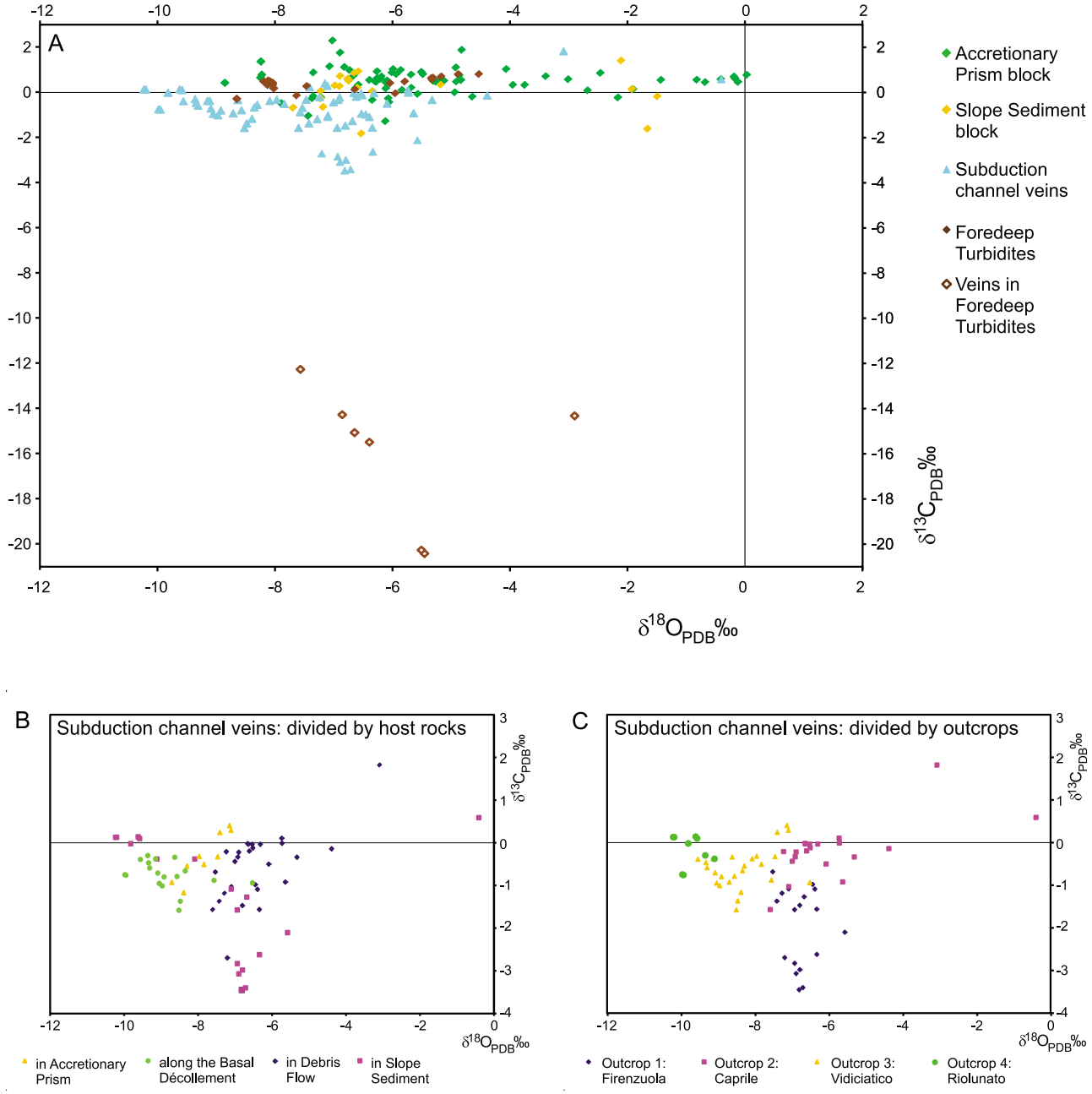

Figure 7. (a) A δ^{13}C (‰PDB) versus δ^{18}O (‰PDB) diagram for the data on all four outcrops. (b) A δ^{13}C (‰PDB) versus δ^{18}O (‰PDB) diagram comparing the veins developed in the different components of the subduction channel. (c) δ^{13}C (‰PDB) versus δ^{18}O (‰PDB) diagram comparing the veins developed in the sampled outcrops along the subduction channel.

fluids containing a heavier δ^{13}C component (Figure 9) consistent with a methanogenic environment.

[62] In summary, Figures 7a and 7b depict several general trends in δ^{18}O and δ^{13}C values: SCVs commonly have both lower δ^{18}O values than their source rocks and negative δ^{13}C values (especially for outcrop 1; Figure 8a). Figure 8 confirms that, with the exception of the Firenzuola outcrop, each locality follows the trend described above, with a clear shift of δ^{18}O and δ^{13}C toward negative values. The progressive decrease in δ^{18}O corresponds to a transition from shallower to deeper levels in the subduction zone (Figure 7c). The most negative values are found along the basal décollement.

6. Discussion

[63] The high number of veins developed during the subduction channel activity implies that the subduction of the Adriatic plate under the European plate was associated with fluid circulation. This occurrence offers the possibility of investigating the hydrological system of an erosive subduction channel. Next we examine this subject from the

Table 1. Summary of Results for Oxygen and Carbon Isotope Distributions in the Four Analyzed Outcrops

Sample Number	Provenance	δ^{18}O PDB[a]	δ^{13}C PDB
Station 1: Firenzuola			
SIL 02	Accretionary prism block: wall rock	−3.39	0.72
BAP LIG CIN 01	Accretionary prism block: vein	−5.86	0.99
BAP LIG CIN 02	Accretionary prism block: vein	−4.82	1.88
BAP LIG CIN 03	Accretionary prism block: vein	−8.23	0.78
BAP LIG CIN 04	Accretionary prism block: vein	−7.02	2.29
BAP LIG CIN 05	Accretionary prism block: vein	−7.35	0.88
BAP LIG CIN 06	Accretionary prism block: vein	−8.24	0.66
BAP LIG CIN 07	Accretionary prism block: vein	−6.89	1.76
FIU 01	slope sediment block: wall rock	−1.66	−1.61
FIU 02	slope sediment block: wall rock	−1.49	−0.17
MMA 01	slope sediment block: wall rock	−1.92	0.15
BAP SV T 01	Subduction channel vein in debris flow	−7.42	−1.37
BAP SV T 02	Subduction channel vein in debris flow	−7.53	−0.68
BAP SV T 03	Subduction channel vein in debris flow	−7.21	−2.70
BAP SV T 04	Subduction channel vein in debris flow	−6.45	−0.98
BAP SV T 05	Subduction channel vein in debris flow	−6.39	−1.09
BAP SV T 06	Subduction channel vein in debris flow	−6.34	−1.56
BAP SV T 07	Subduction channel vein in debris flow	−6.80	−1.47
BAP SV T 08	Subduction channel vein in debris flow	−7.28	−1.19
FIU SV T 01	Subduction channel vein in slope sediment	−6.9	−3.07
FIU SV T 02A	Subduction channel vein in slope sediment	−6.34	−2.62
FIU SV T 02B	Subduction channel vein in slope sediment	−6.82	−3.45
FIU SV T 04	Subduction channel vein in slope sediment	−6.72	−3.40
FIU SV T 06	Subduction channel vein in slope sediment	−5.58	−2.10
FIU SV T 07	Subduction channel vein in slope sediment	−6.94	−2.83
FIU SV T 08	Subduction channel vein in slope sediment	−6.68	−1.27
FIU SV T 09	Subduction channel vein in slope sediment	−6.94	−1.57
FIU SV E 01	Subduction channel vein in slope sediment	−6.8	−2.98
MMA SV T 01	Subduction channel vein in slope sediment	−7.10	−1.09
TCA SV BAR 01	Foredeep turbidite: vein	−6.86	−14.26
TCA SV BAR 03	Foredeep turbidite: vein	−5.84	−26.98
TCA 03	Foredeep turbidite: vein	−2.90	−14.32
TCA SV T 01	Foredeep turbidite: vein	−7.57	−12.26
TCA SV T 02	Foredeep turbidite: vein	−6.64	−15.06
TCA SV E 03	Foredeep turbidite: vein	−5.46	−20.41
TCA SV E 04	Foredeep turbidite: vein	−5.51	−20.26
TCA SV E 05	Foredeep turbidite: vein	−6.39	−15.48
Station 2: Caprile			
APA01	Accretionary prism block: wall rock	−4.64	−0.19
APA02	Accretionary prism block: wall rock	−5.99	1.03
APA03	Accretionary prism block: wall rock	−5.93	0.81
APA04	Accretionary prism block: wall rock	−6.26	0.93
APA05	Accretionary prism block: wall rock	−5.30	0.52
APA06	Accretionary prism block: wall rock	−4.06	1.03
APA08	Accretionary prism block: wall rock	−5.51	0.91
APA09	Accretionary prism block: wall rock	−5.3	0.51
APA10	Accretionary prism block: wall rock	−5.12	0.51
APA11	Accretionary prism block: wall rock	−4.83	0.54
APA12	Accretionary prism block: wall rock	−6.27	0.48
APA13	Accretionary prism block: wall rock	−3.95	0.33
APA14	Accretionary prism block: wall rock	−4.91	0.48
APA15	Accretionary prism block: wall rock	−5.84	0.11
APA16	Accretionary prism block: wall rock	−6.2	0.6
APA17	Accretionary prism block: wall rock	−5.68	0.2
APA18	Accretionary prism block: wall rock	−4.92	1.1
APA19	Accretionary prism block: wall rock	−5.26	0.47
APA20	Accretionary prism block: wall rock	−3.75	0.33
APA21	Accretionary prism block: wall rock	−6.26	0.64
APA22	Accretionary prism block: wall rock	−5.68	0.79
BAP LIG S 03	Accretionary prism block: veins	−1.90	0.14
BAP LIG S 04	Accretionary prism block: veins	−1.43	0.55
BAP LIG S 05	Accretionary prism block: veins	−5.22	0.53
BAP LIG S 06	Accretionary prism block: veins	−6.11	0.18
BAP LIG S 09	Accretionary prism block: veins	−8.85	0.43
BAP LIG S 12	Accretionary prism block: veins	−4.86	0.75
BAP LIG S 14	Accretionary prism block: veins	−6.19	0.70
BAP LIG B 01	Accretionary prism block: veins	−0.82	0.56
BAP LIG B 02	Accretionary prism block: veins	−6.09	0.52
BAP LIG B 03	Accretionary prism block: veins	−5.48	0.80
BAP LIG B 04	Accretionary prism block: veins	−7.21	−0.24

Table 1. (continued)

Sample Number	Provenance	δ^{18}O PDB[a]	δ^{13}C PDB
BAP LIG B 05	Accretionary prism block: veins	−6.01	0.89
BAP LIG B 06	Accretionary prism block: veins	−7.43	−1.04
BAP LIG B 07	Accretionary prism block: veins	−0.12	0.46
BAP LIG B 08	Accretionary prism block: veins	−2.68	0.09
BAP LIG B 09	Accretionary prism block: veins	−6.07	−0.26
BAP LIG E 10	Accretionary prism block: veins	−6.06	−0.44
BAP LIG E 11	Accretionary prism block: veins	−6.62	0.21
BAP LIG E 12	Accretionary prism block: veins	−6.74	0.57
BAP LIG E 13	Accretionary prism block: veins	−7.36	−0.26
BAP LIG E 14	Accretionary prism block: veins	−0.41	0.59
BAP LIG E 15	Accretionary prism block: veins	−0.17	0.62
BAP LIG E 16	Accretionary prism block: veins	−0.68	0.45
BAP LIG E 17	Accretionary prism block: veins	−0.19	0.7
BAP LIG E 18	Accretionary prism block: veins	−6.66	0.74
BAP LIG E 19	Accretionary prism block: veins	0.03	0.77
BAP LIG E 20	Accretionary prism block: veins	−6.11	0.45
BAP LIG E 21	Accretionary prism block: veins	−5.57	−0.07
BAP LIG E 22	Accretionary prism block: veins	−2.46	0.86
BAP LIG E 23	Accretionary prism block: veins	−6.34	−0.34
BAP LIG E 24	Accretionary prism block: veins	−3.01	0.58
BAP SV T 15	Subduction channel vein in debris flow	−6.64	−0.03
BAP SV T 16	Subduction channel vein in debris flow	−5.73	−0.01
BAP SV T 17	Subduction channel vein in debris flow	−7.1	−1.03
BAP SV T 18	Subduction channel vein in debris flow	−5.33	−0.34
BAP SV T 19	Subduction channel vein in debris flow	−7.24	−0.21
BAP SV T 20	Subduction channel vein in debris flow	−6.92	−0.33
BAP SV T 21	Subduction channel vein in debris flow	−6.52	−0.12
BAP SV T 22	Subduction channel vein in debris flow	−6.62	−0.19
BAP SV T 22bis	Subduction channel vein in debris flow	−6.54	−0.04
BAP SV T 23	Subduction channel vein in debris flow	−4.39	−0.14
BAP SV T 24	Subduction channel vein in debris flow	−6.9	−0.22
BAP SV T 25	Subduction channel vein in debris flow	−6.66	−0.02
BAP SV T 26	Subduction channel vein in debris flow	−3.09	1.82
BAP SV T 27	Subduction channel vein in debris flow	−5.74	0.11
BAP SV T 28	Subduction channel vein in debris flow	−6.32	−0.03
BAP SV T 29	Subduction channel vein in debris flow	−7.00	−0.44
BAP SV T 29bis	Subduction channel vein in debris flow	−6.09	−0.5
BAP SV T 30	Subduction channel vein in debris flow	−7.6	−1.57
BAP SV T 31	Subduction channel vein in debris flow	−5.64	−0.92
BAP CIV E 14	Subduction channel vein in slope sediment	−0.41	0.59
Station 3: Vidiciatico			
SV 01	Accretionary prism block: wall rock	−7.89	−0.48
AVC 01	Accretionary prism block: wall rock	−6.73	0.99
AVC 02	Accretionary prism block: wall rock	−6.82	1.12
AVC 02A	Accretionary prism block: wall rock	−6.39	0.55
AVC 03	Accretionary prism block: wall rock	−6.58	0.33
AVC 04	Accretionary prism block: wall rock	−7.07	1.15
AVC 05	Accretionary prism block: wall rock	−7.35	−0.16
AVC 06	Accretionary prism block: wall rock	−6.29	0.48
AVC LIG E 01	Accretionary prism block: vein	−8.24	1.37
AVC LIG E 02	Accretionary prism block: vein	−6.12	−1.28
AVC LIG CIN 01	Accretionary prism block: vein	−2.16	−0.23
AVC LIG CIN 02	Accretionary prism block: vein	−4.94	0
CNG 1	slope sediment block: wall rock	−2.11	1.41
MMA 03	slope sediment block: wall rock	−7.69	−0.68
FLP 01	slope sediment block: wall rock	−6.53	−1.82
CIV 02	slope sediment block: wall rock	−7.18	−0.65
CIV 03	slope sediment block: wall rock	−7.22	−0.27
CIV SV T 01	Subduction channel vein in slope sediments	−8.09	−0.38
AVC SV T 01	Subduction channel vein in accretionary prism block	−8.3	−0.55
AVC SV T 02	Subduction channel vein in accretionary prism block	−8.39	−1.17
AVC SV T 01bis	Subduction channel vein in accretionary prism block	−8.71	−0.93
AVC SV T 02bis	Subduction channel vein in accretionary prism block	−7.84	−0.51
AVC SV T 03	Subduction channel vein in accretionary prism block	−7.47	−0.33
AVC SV T 04	Subduction channel vein in accretionary prism block	−7.97	−0.32
AVC SV T 04bis	Subduction channel vein in accretionary prism block	−7.11	0.29
VC SV T 05	Subduction channel vein in accretionary prism block	−7.15	0.4
AVC SV T 06	Subduction channel vein in accretionary prism block	−7.41	0.24
CEV/MMA SV T 01	Subduction channel vein along lower décollement	−9.09	−0.71
CEV/MMA SV T 02	Subduction channel vein along lower décollement	−9.56	−0.39
CEV/MMA SV T 03	Subduction channel vein along lower décollement	−9.05	−0.95

Table 1. (continued)

Sample Number	Provenance	δ^{18}O PDB[a]	δ^{13}C PDB
CEV/SV SV T 01	Subduction channel vein along lower décollement	−8.92	−0.8
FLP/CIV SV T 01	Subduction channel vein along lower décollement	−7.57	−0.88
FLP/CIV SV T 02	Subduction channel vein along lower décollement	−6.53	−0.94
FLP CIV SV T 03	Subduction channel vein along lower décollement	−8.63	−0.34
CEV/MMA SV E 01	Subduction channel vein along lower décollement	−8.48	−1.37
CEV/MMA SV E 02	Subduction channel vein along lower décollement	−9.31	−0.59
CEV/MMA SV E 03	Subduction channel vein along lower décollement	−9.34	−0.47
FLP/CIV SV E 01	Subduction channel vein along lower décollement	−8.52	−1.58
FLP/CIV SV E 02	Subduction channel vein along lower décollement	−8.57	−0.79
FLP/CIV SV E 03	Subduction channel vein along lower décollement	−8.35	−0.66
FLP/CIV SV E 04	Subduction channel vein along lower décollement	−8.97	−1.01
FLP/CIV SV E 05	Subduction channel vein along lower décollement	−9.15	−0.38
Station 4: Riolunato			
MMA 100	Slope sediment block	−6.58	0.92
MMA 102	Slope sediment block	−6.65	0.86
MMA 103	Slope sediment block	−6.74	0.51
MMA 104	Slope sediment block	−6.6	0.2
MMA 105	Slope sediment block	−6.75	0.55
MMA 106	Slope sediment block	−6.76	0.61
MMA 107	Slope sediment block	−6.9	0.27
MMA 109a	Slope sediment block	−6.98	0.31
MMA 109	Slope sediment block	−6.89	0.72
SCAR 1	Slope sediment block	−5.18	0.34
SCAR 2	Slope sediment block	−7.22	0.06
SCAR 3	Slope sediment block	−6.34	0.06
SER 1	Foredeep turbidites (Burdigalian)	−6.04	0.4
SER 2	Foredeep turbidites (Burdigalian)	−5.34	0.64
SER 3	Foredeep turbidites (Burdigalian)	−4.53	0.81
SER 4	Foredeep turbidites (Burdigalian)	−5.79	0.48
SER 5	Foredeep turbidites (Burdigalian)	−4.88	0.81
SER 8	Foredeep turbidites (Burdigalian)	−5.32	0.56
SER 9	Foredeep turbidites (Burdigalian)	−5.31	0.65
SLT 01	Foredeep turbidites (Burdigalian)	−7.46	0.28
SLT 02	Foredeep turbidites (Burdigalian)	−8.65	−0.28
SLT 03	Foredeep turbidites (Burdigalian)	−6.64	0.13
SLT 05	Foredeep turbidites (Burdigalian)	−7.63	−0.14
SLT 06	Foredeep turbidites (Burdigalian)	−5.95	−0.04
SLT 07	Foredeep turbidites (Burdigalian)	−5.17	0.7
MOD 1	Foredeep turbidites (Chattian Aquitanian)	−8.19	0.49
MOD 2	Foredeep turbidites (Chattian Aquitanian)	−8.09	0.5
MOD 3	Foredeep turbidites (Chattian Aquitanian)	−8.1	0.42
MOD 4	Foredeep turbidites (Chattian Aquitanian)	−8.04	0.43
MOD 5	Foredeep turbidites (Chattian Aquitanian)	−8.13	0.34
MOD 6	Foredeep turbidites (Chattian Aquitanian)	−8.12	0.52
MOD 7	Foredeep turbidites (Chattian Aquitanian)	−8.04	0.35
MOD 8	Foredeep turbidites (Chattian Aquitanian)	−8.02	0.19
MOD SV T01	Subduction channel vein along lower décollement	−9.98	−0.75
MOD SV T02	Subduction channel vein along lower décollement	−9.95	−0.76
MOD SV T03	Subduction channel vein along lower décollement	−9.36	−0.3
MMA SV T100	Subduction channel vein in slope sediment	−10.2	0.13
MMA SV T101	Subduction channel vein in slope sediment	−9.11	−0.38
MMA SV T102	Subduction channel vein in slope sediment	−9.62	0.14
MMA SV T103	Subduction channel vein in slope sediment	−10.23	0.13
MMA SV T104	Subduction channel vein in slope sediment	−9.82	−0.02
SCAR SV T01	Subduction channel vein in slope sediment	−9.58	0.1

[a]PDB, Peedee belemnite.

perspectives of structural analysis of veins and associated deformation in host rock and the stable isotope composition of carbonate veins.

6.1. Strain Evolution and Associated Conditions for Vein Deposition

[64] The Apennine subduction channel is characterized by both high lithological variability and entrance of material at markedly different stages of lithification. Blocks of Late Cretaceous-early Eocene accretionary prism, already well lithified and deformed, were entering the channel together with unlithified, newly deposited slope sediments and debris flows. This high heterogeneity influenced strain localization, at least during the early stages and shallower portions of subduction channel activity. In the shallow portions of the subduction channel, strain is localized in slope sediments and debris flows. In this region veins did not form, despite evidence from the great deal of compaction that fluids were

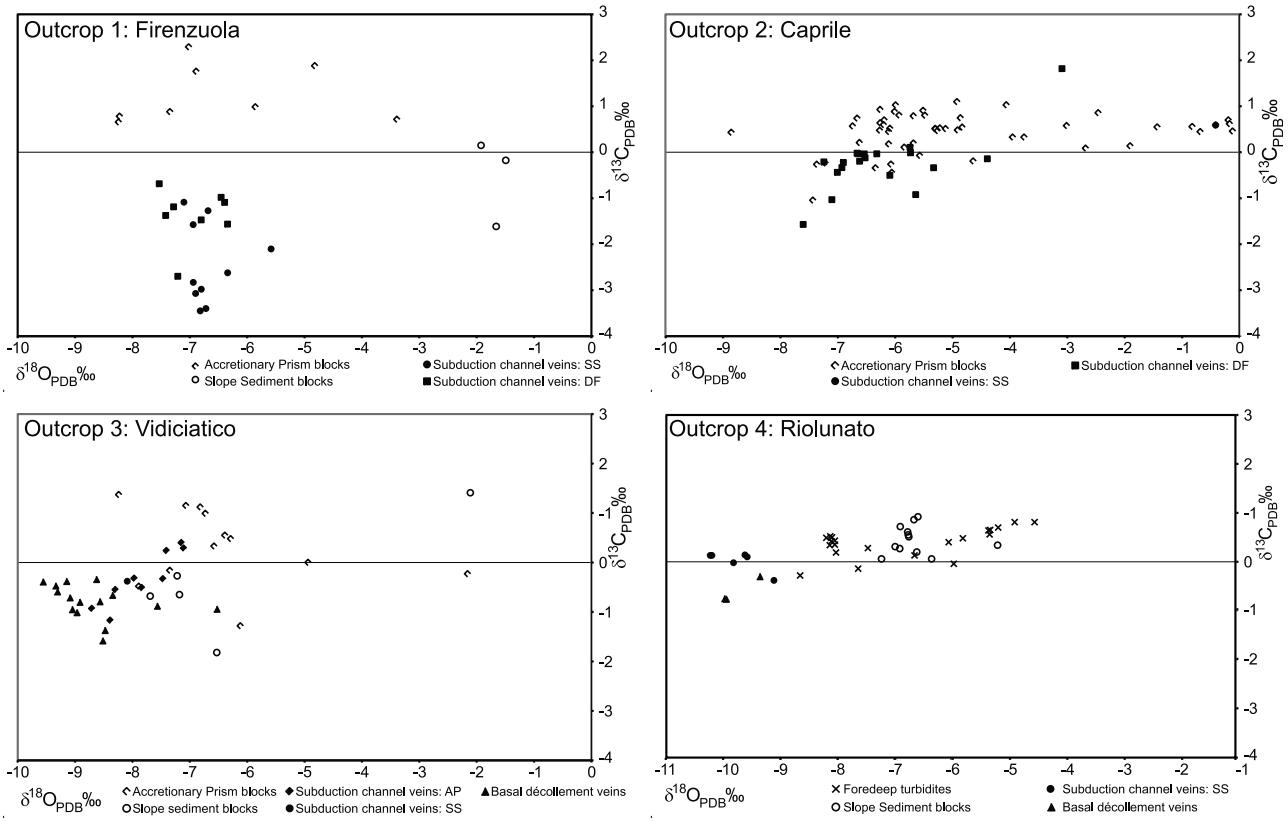

Figure 8. $\delta^{13}C$ (‰PDB) versus $\delta^{18}O$ (‰PDB) diagrams for the data on each outcrop. For each outcrop, wall rock, and veins were separated. The figure also marks which component of the subduction channel was sampled and the nature of the sampled vein wall rock. AP, Late Cretaceous-early Eocene accretionary prism component; DF, debris flow component; SS, slope sediment component.

abundant and that strain was also accommodated through failure. The unlithified sediment seems to have been too weak to sustain fluid pressure drops as shown by the continuous occurrence of new fracture episodes, which most likely developed as soon as the sediment strain-hardened. Sandstones are the first sediment type to host veins; their extensional texture implies a considerable cohesive strength of the fractured rock. Cohesion, in turn, implies at least partial cementation of the sand, suggesting that lithification was easiest and quickest in permeable rocks.

[65] This shallower portion of the subduction channel, despite being a megashear zone in a compressive geodynamic environment, was characterized by extensional deformation. The conjugate sets of normal faults imply that the maximum principal stress, σ_1, was vertical. Extension along the shallow portion of compressive plate boundaries or in the upper plate is also indicated by observations in modern subduction zones [*Sage et al.*, 2004; *Vannucchi and Leoni*, 2007; *Lewis et al.*, 2008].

[66] Extensional modes of deformation persisted in the intermediate portion of the subduction channel, where strain involved all the components of the channel and shear surfaces were active at 50°–80° to σ_1 (Figure 4e). The geometry of the crack-and-seal extensional veins (Figures 5a and 5b) suggests that the maximum principal stress was oriented at a high angle, that is, subvertical, to the bounding shear surfaces. The crack-and-seal texture is also present in the dilational stopovers, where extensional veins have an internal fabric similar to that in Figures 5a and 5b. The crack-and-seal portions of striped veins can be considered small dilational stepovers since they are bounded by parallel shear surfaces.

[67] A subvertical maximum principal stress within the shear zones is "unfavorably" oriented with respect to the far-field driving stress; this defines the shear zones to have been weak faults. This result is further constrained by the small extensional veins developed in the shales and the constant action of pressure solution within the veins (Figures 4e, 5c, and 5d).

[68] As suggested by *Ramsay* [1980] and *Ramsay and Huber* [1983], the regular periodicity shown by crack-and-seal veins is induced by hydraulic fracturing under cyclic changes of pore pressure. In this case the dark shear surfaces connected high-angle to subvertical extensional veinlets that opened up parallel to σ_3. This requires an increase in fluid pressure above σ_3 and a low differential stress along the shear surfaces. The achievement of failure conditions is then followed by a drop in fluid pressure until sealing reoccurs.

[69] Deactivation and sealing are indicated by normal faults that cut the well-exposed basal décollement (Figure 4d). This demonstrates its locking at intermediate depths, while slip migrating to other, subparallel shear surfaces within the channel, following a general trend of upward migration of the active shear zone.

Table 2. Data Averages Calculated for $\delta^{13}C$ and $\delta^{18}O$ for the Different Components of the Subduction Channel

Outcrop and Nature of Samples	Component	Average $\delta^{18}O$	Average $\delta^{13}C$	Δx (=δx Veins of Subduction Channel Phase − δx Source Rock)	
				$\Delta^{18}O$	$\Delta^{13}C$
Station 1: Firenzuola					
Source rock	Accretionary prism	−6.48	1.25	−0.31	−3.22
Source rock	Slope deposit	−1.69	−0.55	−5.1	−1.42
Veins	Subduction channel	−6.79	−1.97		
Station 2: Caprile					
Source rock	Accretionary prism	−4.74	0.44	−0.60	−0.76
Veins	Subduction channel	−5.92	−0.18		
Station 3. Vidiciatico					
Source rock	Accretionary prism	−6.38	0.32	−1.96	−0.93
Source rock	Slope deposit	−6.15	−0.40	−2.19	−0.21
Veins	Subduction channel	−8.34	−0.61		
	i. In the channel	−7.81	−0.32		
	ii. At the contact	−8.67	−0.79		
Station 4. Riolunato					
Source rock	Slope deposit	−6.63	0.45	−3.13	−0.64
Veins	Subduction channel	−9.76	−0.19		
	i. In the channel	−9.76	0.02		
	ii. At the contact	−9.76	−0.60		
Source rock	Foredeep	−6.83	0.39	−2.93	−0.58

[70] Crack-and-seal growth is followed by brecciated calcite, especially in the dilational jogs. Brecciation has been classically related either to cataclastic friction during shearing or to hydraulic fracturing related to high fluid pressure. An alternative mechanism could be the drop of fluid pressure inside the jog below the level of the fluid pressure in the surrounding rock, with the subsequent formation of an implosion breccia [*Sibson*, 2001]. Here the latter mechanism is suggested by the lack of block rotation and shearing typical of cataclasis. The breccia is also always confined by shear surfaces not involved in the brecciation itself, as would be expected for hydrofracturing. The observed structures are, instead, in agreement with a sudden increase in the volume of the vein. These dilational jogs are related to the rupture associated with slip along a fault as reported by *Okamoto et al.* [2006]. Field exposure of dilational jogs, in fact, has been related to a seismogenic behavior of fault systems under conditions of high fluid pressure [*Micklethwaite and Cox*, 2006]. The lack of other significant microstructures constrains the development of the breccias to a single episode.

[71] This structural analysis of the veins leads to the following conclusions.

[72] 1. During the opening of the extensional veins the shear surface acted like a weak fault, therefore propagation of the extensional vein across the surfaces was prevented.

[73] 2. Outside of the crack-and-seal portions of the stripes and dilational stepovers, the condition for extensional-shear failure was not reached. Discontinuous crack-and-seal growth is present in veins cutting through the different components of the subduction channel when they reached an appropriate cohesive strength.

[74] 3. During fracture mineralization the mechanics of deformation inside the veins evolved drastically, and the discontinuous but regular periodic release of elastic deformation and failure was replaced by implosion into transient voids. At this stage failure connected areas with higher and lower fluid pressure, which was balanced by rapid fluid flow. Fluid pressure dropped below the fluid pressure in surrounding rock [*Sibson*, 2000], and the propagation of the movement along the faults stopped, contributing to its locking.

[75] The investigation of the causes of the weakening mechanisms operating within the subduction channel is not the primary scope of the present paper. Nonetheless, we can state a few ideas that could help address future research on the causes of the inferred fault weakness, keeping in mind that the exhumed portions of this fault have their maximum load-bearing region at a depth of ~5 km. In the subduction channel the introduction of unlithified material facilitated fluid influx into the active fault zone. Faulting within the subduction channel produced high interconnectivity that could quickly and effectively link weak layers. The dark shear surfaces of the calcite veins, in fact, connected subvertical extension veinlets, creating a situation where shear occurred by extension under local hydrofracture conditions between weak planes. On the contrary, the impermeable character of the clay-rich layers and of the shear zones (as they transferred fluids from a channel deeper down) facilitated more transient weakening effects due to the local short-lived overpressure of fluid, which led to hydrofracturing and mineralization.

6.2. Fluid Source and Fluid-Rock Interaction

[76] As discussed in the previous section, fluids influence the mechanisms of deformation inside the subduction channel and can control the upward migration of the shear zone. The geochemistry of erosive subduction systems has been investigated only in modern subduction zones, that is,

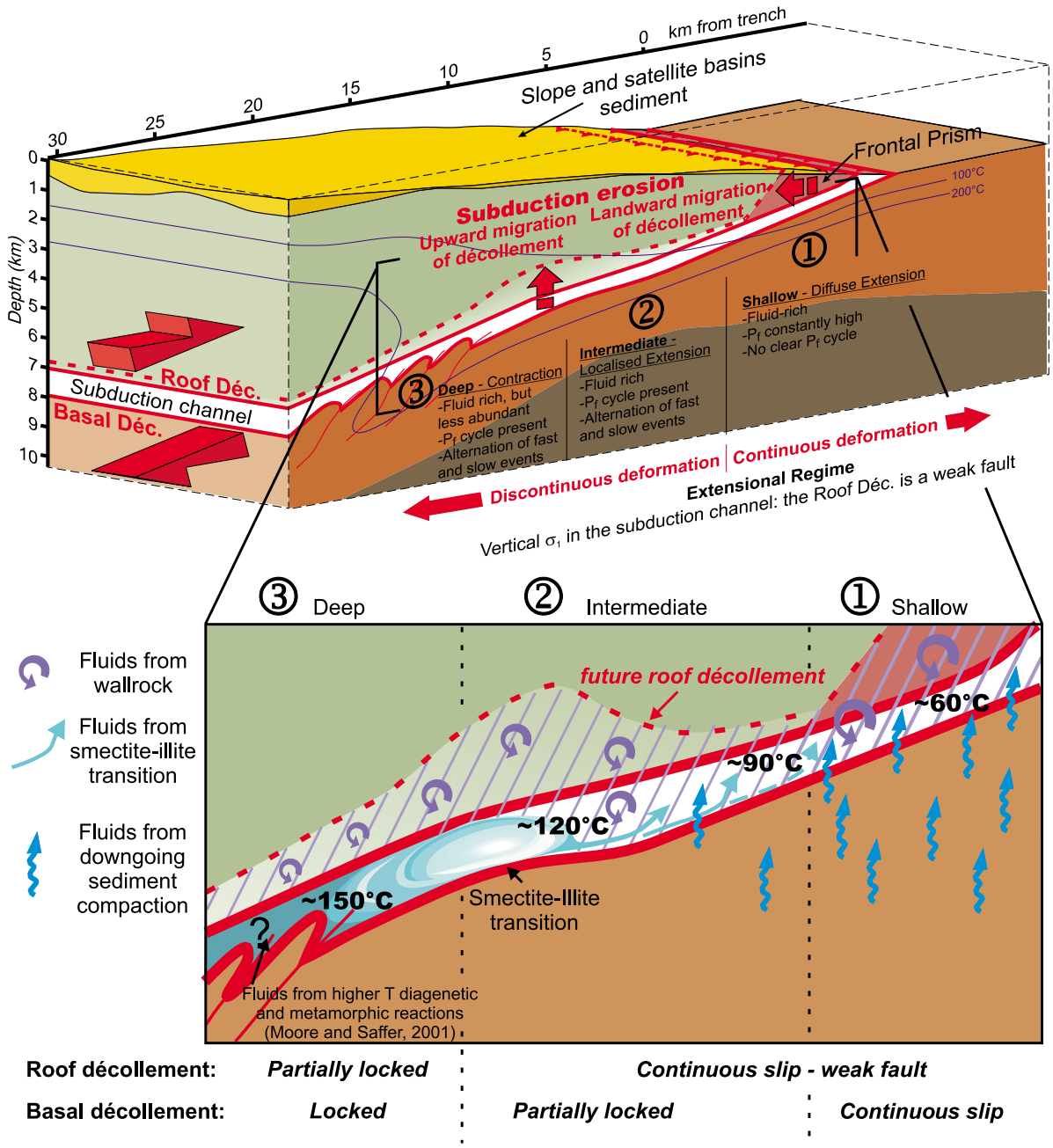

Figure 9. Scheme of a conceptual model of the deformation and geochemical system of an erosive subduction channel. Isotherms are taken from the well-studied erosive Costa Rica margin [*Harris and Wang*, 2002; *Ranero et al.*, 2008], integrated with thermal constraints from the Apennine subduction channel.

Costa Rica [*Silver et al.*, 2000; *Wei et al.*, 2008], while this study represents the first study of a fossil system.

[77] Possible end members for the possible sources of the fluids producing the O isotopic composition of the calcite veins (Figure 7) are as follows: (1) the circulating fluids come from fluid contained in the sediment pores (i.e., subducted pore water) or are liberated by early dehydration reactions; (2) internal/external fluids are buffered by the surrounding host rocks; and (3) fluids are externally derived, migrating along the décollement toward the deformation front, and are not in isotope equilibrium with the host rocks. Choosing between these hypotheses (internal/exotic fluids origin and localized/pervasive source) is critical for developing the correct model of fluid flow in this geological context. However, neither the exact temperature nor the oxygen isotopic composition of the fluid from which calcite precipitated is known, and this causes the ^{18}O data to be somewhat ambiguous. Here, we discuss these different hypotheses on the basis of literature data and with the assumption that veins formed in the temperature range of 80°–130°C as inferred from data on the maturity of organic matter, clay mineral assemblages, and thermocronology

[*Reutter et al.*, 1992; *Zattin et al.*, 2000; *Carlini et al.*, 2009].

[78] Most pore waters recovered from shallow sediments are within ±3‰ seawater value (seawater $\delta^{18}O$ is by definition $0‰_{SMOW}$ [*Kastner et al.*, 1991]). While it is unlikely that a pore fluid would remain for a long time without any exchange with the surrounding rocks, a fluid with an isotopic composition similar to that of seawater could remain if a relatively large amount of pore water was retained in these rocks and relatively little exchange took place between the pore water and surrounding rocks until veins were precipitated [*Sadofsky and Bebout*, 2004]. In that case the expected O isotope composition of $CaCO_3$ veins formed in equilibrium with a seawater-like fluid (fractionation factors from *O'Neil et al.* [1969]) at a temperature compatible with the structural studies (about 80°–130°C) is about −12‰/−17‰ PDB, much more negative than what we find (Figure 7).

[79] The second hypothesis is that an internal/external fluid is partially or entirely rock buffered in its isotopic composition. Such a condition does not allow determination of a fluid source(s) but only indicates that the fluid equilibrated with the host rocks (or lithologies similar to host rocks) and that any infiltration by externally derived fluid initially out of isotopic equilibrium with the host rocks was insufficient to change the isotopic composition of the rock. In this case, if fluids are buffered by the enclosing rocks, the $\delta^{18}O$ of the newly precipitated calcite veins will be nearly equal to the values of the host rocks. Our results do not confirm this hypothesis, highlighting that the $\delta^{18}O$ values of the SCVs are lower than those of their host rocks.

[80] Alternatively, a relatively large volume of external fluids (i.e., a high water/rock ratio) could buffer the isotopic compositions of the veins. This would probably come from depth, where several low-grade metamorphic reactions release chemically bound water [*Moore and Saffer*, 2001]. The Apennine plate boundary megathrust would channel fluids from depth, as has been argued for fluid flow in modern subduction zones [*Silver et al.*, 2000; *Moore et al.*, 2001]. The principal sources of fluids are usually identified to be the biogenic opal-quartz transformation that occurs at a temperature of ~50°–100°C and the smectite-illite reaction that occurs at a temperature of 120°–150°C [*Moore and Vrolijk*, 1992]. In the study area the material involved in the subduction channel does not contain biogenic opal, while quartz is of detrital origin; for this reason, the smectite-illite transformation appears to be the most probable source of fluids. A pilot study on the thermal constraints of the Apennine subduction channel indicates the illite percentage in illite-smectite mixed layers to range between 80% and 90% and the Kübler Index to be between 0.63 and 0.77 [*Carlini et al.*, 2009]. Ca-montimorillonite, the probable smectite mineral in accretionary prism sediments, contains 10%–20% water, by weight: water that is completely liberated when smectite dissolves and illite precipitates. This water release could also potentially lead to substantial transient overpressures [*Moore and Vrolijk*, 1992].

[81] The oxygen isotopic value of interstitial water is supposed to be increased by clay dehydratation reactions [*Elderfield et al.*, 1990; *Vrolijk et al.*, 1990]; the degree of the enrichment would depend on the amount of interlayer water that was expelled.

[82] Loss of interlayer water from smectites may be a key process in generating fluids enriched in $\delta^{18}O$ (in comparison with the average value of the original pore fluids) that subsequently migrates along the décollement zone. Those fluids precipitated calcite veins with distinct $\delta^{18}O$ values (Figure 7), which depend on the precipitation temperature (i.e. depth of precipitation): at higher temperatures, about 120°–150°C (outcrops Vidiciatico and Riolunato; Figure 7c), the $\delta^{18}O$ value of carbonate veins would be more negative (closer to the $\delta^{18}O$ fluid value) than at lower temperatures (outcrop Caprile; Figure 7c), owing to an inverse correlation of temperature and fractionation (i.e., more fractionation at lower temperatures). The veins collected along the basal décollement show the most negative $\delta^{18}O$ values, which supports the idea that the basal décollement was a main, rather continuous shear surface that could collect hot modified fluids from depth.

[83] On the contrary, the relatively narrow range of $\delta^{13}C$ values of the SCVs are inconsistent with normal marine carbonates, that is, between −2‰ and +4‰ [*Hoefs*, 1997; *Baumgartner and Valley*, 2001], in equilibrium with the local host rocks.

[84] In summary, the oxygen isotope composition of calcite veins is compatible with the influence from fluids released by smectite dewatering at depth. The transport distance for deep-sourced fluids is difficult to estimate, but it can reasonably be inferred to be of the order of a few kilometers based on data from modern subduction zones [*Silver et al.*, 2000; *Moore et al.*, 2001]. Carbon isotope compositions reveal a subsequent interaction with the carbon-bearing host rocks.

[85] Overall, isotopic studies of the SCVs and host rocks reveal a complex hydrogeological model where channeled modified pore fluids coming from depth locally interacted with host rocks in the subduction channel, at different temperatures and depths, which produced a range of compositionally distinct carbonate veins. Locally, fluids coming from the underthrusting foredeep turbidites affected the carbon isotopic composition of the veins, which suggests a methanogenic environment.

7. Conclusions

[86] The observations described in this paper lead to several conclusions about the pattern, scale, and temperature of fluid-rock interactions and the source of fluids involved in an erosive subduction channel. The orientation patterns and crosscutting relationships among the structures developed in the erosive subduction channel imply an evolution of the deformation as the material was transported to deeper and hotter portions of the channel. The dominant preserved deformation regime inside the shallowest subduction channel is extensional. Alternation with compressional events is present; this effect grows as the deeper parts of the channel are approached. Extensional deformation implies a vertical maximum principal stress σ_1, that is, sub-perpendicular to the plate boundary, which means that the plate boundary mostly behaved as a weak fault. In the case of the subduction channel the plate boundary is characterized by several subparallel décollements, with two of them, at the top and at the bottom, easy to identify. While the basal décollement

permitted extension to deform the subduction channel material, the basal décollement also worked as a barrier to penetration of extensional deformation. This observation implies that the roof behaved as a weak fault, while the basal décollement had a different mechanical character.

[87] Normal faults cut the basal décollement in the intermediate zone. These show that the décollement was deactivated, implying that the lower part of the subduction channel was stronger by this stage. The evidence that deformation was becoming more active at the top of the subduction channel is in agreement with an upward-migrating décollement typical of subduction erosion. At the mesoscale the rheology of the material involved in the subduction channel evolves from viscoelastic in the shallow zone to elastic in the intermediate and deep zone. The onset of fault-like failure is linked to cyclical rise and drop of fluid pressure. The subduction channel material in the intermediate zone can accumulate fluid pressure until the tensile overpressure condition ($P_f > \sigma_3$) is reached locally. As deeper portions of the outcropping Apennine subduction channel are approached, this cyclical, self-similar movement propagation is no longer observed. Instead, there are more common dilational jogs. These features appear to represent the transition from an aseismic to a seismic behavior of the décollement.

[88] The mechanical behavior of the subduction channel is linked to fluids. Patterns of deformation structures indicate a progressive homogenization of the rheology of the subduction channel components as they progressively consolidate. Three main fluid sources have been identified. While in situ fluids in equilibrium with the subduction channel components were found at all sites, in addition, fluids from the underthrusting foredeep turbidites and fluids from depth have a significant influence in different portions of the subduction channel. In the shallow part of the intermediate zone the mineralizing fluids mainly come from the underthrusting and subsequent dewatering of foredeep turbidites. In the deeper portions of the subduction channel, in particular, along the basal décollement, fluids come from diagenetic/low-metamorphism reactions. The presence of resident fluids, coming from the subduction channel components eroded from the upper plate, implies a partial recycling of fluids accompanying the solid phase.

[89] The progressive increase in the deep fluid signature as the deeper portions of the subduction channel are approached involves a complex fracture/fault system where fluid flow episodes must have either been highly channelized or had restricted pathways to maintain the recorded isotopic heterogeneities.

[90] The basal décollement and related faults did not function in the subduction channel as permanently weak shear zones. Instead, they show evidence of having progressively stopped their activity. Despite the important role of the basal décollement within the subduction channel, it did not evolve into a mature fault zone and its position did not remain fixed in space. Permanent weakening, as triggered, for example, by alteration of mineral phases, did not play a prominent role in this shallow part of the Apennine subduction channel. Instead, weakening was linked to direct fluid influx into active faults from various sources (Figure 9).

[91] **Acknowledgments.** The authors would like to thank associate editor Richard Arculus, David Kirschner, and an anonymous reviewer for helpful suggestions that greatly improved the manuscript. P.V. thanks J. Phipps Morgan for fruitful discussions. C.B. thanks Enrico Calvi for assistance with stable isotope analyses.

References

Abbate, E., V. Bortolotti, and M. Sagri (1981), Excursion N.5: Olistostromes in the Oligocene Macigno formation (Florence area), Introduction: An approach to olistostrome interpretation, in *International Association of Sedimentologists, 2nd European Regional Meeting*, edited by F. Ricci Lucchi, pp. 165–185, Tecnoprint, Bologna.

Audet, P., M. G. Bostock, N. I. Christensen, and S. M. Peacock (2009), Seismic evidence for overpressured subducted oceanic crust and megathrust fault sealing, *Nature*, *457*(7225), 76–78, doi:10.1038/ature07650.

Bangs, N. L. B., T. H. Shipley, J. C. Moore, and G. F. Moore (1999), Fluid accumulation and channeling along the Northern Barbados Ridge decollement thrust, *J. Geophys. Res.*, *104*(B9), 20,399–20,414, doi:10.1029/1999JB900133.

Bangs, N. L., T. H. Shipley, S. P. S. Gulick, G. F. Moore, S. Kuromoto, and Y. Nakamura (2004), Evolution of the Nankai Trough decollement from the trench into the seismogenic zone: Inferences from three-dimensional seismic reflection imaging, *Geology*, *32*(4), 273–276, doi:10.1130/G20211.2.

Baumgartner, L. P., and J. W. Valley (Eds.) (2001), *Stable Isotope Transport and Contact Metamorphic Fluid Flow*, pp. 415–467, Mineralogical Society of America, Chantilly, Va.

Bettelli, G. (2002), Foglio 236 Pavullo nel Frignano e Note Illustrative della Carta Geologica d'Italia alla scala 1:50.000, S.EL.CA., Firenze.

Bettelli, G., and M. Boccaletti (2002), Foglio 252 Barberino nel Mugello e Note Illustrative della Carta Geologica d'Italia alla scala 1:50.000, S.EL.CA., Firenze.

Bettelli, G., and F. Panini (1989), I mélanges dell'Appennino Settentrionale dal T. Tersinaro al T. Sillaro, *Mem. Soc. Geol. Ital.*, *39*, 187–214.

Bettelli, G., and F. Panini (1992), Liguridi, mélanges e tettoniti nel complesso caotico lungo la "linea del Sillaro" (Appennino Settentrionale, Provincie di Firenze e Bologna), *Mem. Descrit. Carta Geol. Ital.*, *39*, 91–125.

Bettelli, G., and P. Vannucchi (2003), Structural style of the offscraped Ligurian oceanic sequences of the Northern Apennines: New hypothesis concerning the development of melange block-in-matrix fabric, *J. Struct. Geol.*, *25*(3), 371–388, doi:10.1016/S0191-8141(02)00026-3.

Bettelli, G., M. Capitani, F. Panini, and M. Pizziolo (1996), Le rocce caotiche dell'Appennino emiliano: Metodi sperimentali di rilevamento stratigrafico, esempi e nomenclatura, *Accad. Nazion. Sci. Lettere Arti Modena, Collana Studi*, *15*, 189–220.

Brown, K. M., D. M. Saffer, and B. A. Bekins (2001), Smectite diagenesis, pore-water freshening, and fluid flow at the toe of the Nankai wedge, *Earth Planet. Sci. Lett.*, *194*(1/2), 97–109, doi:10.1016/S0012-821X(01)00546-5.

Carlini, M., L. Aldega, S. Corrado, P. Vannucchi, F. Remitti, and G. Bettelli (2009), New thermal constraints on a shallow fossil subduction channel from the Northern Apennines of Italy, *Geophysical Research Abstracts, EGU General Assembly*, *11*, EGU2009–EGU9405.

Carson, B., and E. J. Screaton (1998), Fluid flow in accretionary prisms: Evidence for focused, time-variable discharge, *Rev. Geophys.*, *36*(3), 329–351, doi:10.1029/97RG03633.

Cibin, U., E. Spadafora, G. G. Zuffa, and A. Castellarin (2001), Continental collision history from arenites of episutural basins in the Northern Apennines, Italy, Geol. *Soc. Am. Bull.*, *113*(1), 4–19, doi:10.1130/0016-7606(2001)113<0004:CCHFAO>2.0.CO;2.

Clift, P., and P. Vannucchi (2004), Controls on tectonic accretion versus erosion in subduction zones: Implications for the origin and recycling of the continental crust, *Rev. Geophys.*, *42*, RG2001, doi:10.1029/2003RG000127.

Cloos, M., and R. L. Shreve (1988), Subduction-channel model of prism accretion, mélange formation, sediment subduction, and subduction erosion at convergent plate margins, 2: Implications and discussion, *Pure Appl. Geophys.*, *128*(3/4), 501–545, doi:10.1007/BF00874549.

Conti, S., and D. Fontana (2005), Anatomy of seep-carbonates: Ancient examples from the Miocene of the Northern Apennines (Italy), *Palaeogeogr. Palaeoclimatol. Palaeoecol.*, *227*(1–3), 156–175, doi:10.1016/j.palaeo.2005.04.032.

Coward, M. P., and D. Dietrich (1989), Alpine tectonics—an overview, in *Alpine Tectonics*, edited by M. P. Coward, D. Dietrich, and R. G. Park, pp. 1–29, Geological Society, London.

Deng, X. H., and M. B. Underwood (2001), Abundance of smectite and the location of a plate-boundary fault, Barbados accretionary prism, *Geol.*

Soc. Am. Bull., *113*(4), 495–507, doi:10.1130/0016-7606(2001)113<0495:AOSATL>2.0.CO;2.

Elderfield, H., M. Kastner, and J. B. Martin (1990), Compositions and sources of fluids in sediments of the Peru Subduction Zone, *J. Geophys. Res.*, *95*, 8819–8827, doi:10.1029/JB095iB06p08819.

Harris, R. N., and K. Wang (2002), Thermal models of the middle America trench at the Nicoya Peninsula, Costa Rica, *Geophys. Res. Lett.*, *29*(21), 2010, doi:10.1029/2002GL015406.

Hilde, T. W. C. (1983), Sediment subduction versus accretion around the Pacific, *Tectonophysics*, *99*, 381–397, doi:10.1016/0040-1951(83)90114-2.

Hoefs, J. (1997), *Stable Isotope Geochemistry*, Springer-Verlag, Berlin.

Jolivet, L., and C. Faccenna (2000), Mediterranean extension and the Africa-Eurasia collision, *Tectonics*, *19*(6), 1095–1106, doi:10.1029/2000TC900018.

Kastner, M., H. Elderfield, and J. B. Martin (1991), Fluids in convergent margins—What do we know about their composition, origin, role in diagenesis and importance for oceanic chemical fluxes, *Philos. Trans. R. Soc. A*, *335*, 243–259.

Kligfield, R., J. Hunziker, R. D. Dallmeyer, and S. Schamel (1986), Dating of deformation phases using K-Ar and 40Ar/39Ar techniques: Results from the Northern Apennines, *J. Struct. Geol.*, *8*(7), 781–798, doi:10.1016/0191-8141(86)90025-8.

Koehn, D., and C. W. Passchier (2000), Shear sense indicators in striped bedding-veins, *J. Struct. Geol.*, *22*(8), 1141–1151, doi:10.1016/S0191-8141(00)00028-6.

Landuzzi, A. (1994), Relationships between the Marnoso-Arenacea formation of the inner Romagna units and the Ligurids (Italy), *Mem. Soc. Geol. Ital.*, *48*, 523–534.

Le Pichon, X., P. Henry, and S. Lallemant (1993), Accretion and erosion in subduction zones: The role of fluids, *Annu. Rev. Earth Planet. Sci.*, *21*, 307–331, doi:10.1146/annurev.ea.21.050193.001515.

Lewis, J., K. Kanagawa, T. Byrne, V. Famin, J. Behrmann, T. Kanamatsu, and J. Pares (2008), Subhorizontal extension of the upper plate at NantroSEIZE sites C0001 and C0002, *Eos Trans. AGU*, *89*(53), Fall Meet. Suppl., Abstract T31B-2005.

Lewis, K. B., and B. A. Marshall (1996), Seep faunas and other indicators of methane-rich dewatering on New Zealand convergent margins, *N. Z. J. Geol. Geophys.*, *39*(2), 181–200.

Malinverno, A., and W. Ryan (1986), Extension in the Tyrrhenian Sea and shortening in the Apennines as a result of arc migration driven by sinking of the lithosphere, *Tectonics*, *5*, 227–246, doi:10.1029/TC005i002p00227.

Marroni, M., G. Molli, A. Montanini, and R. Tribuzio (1998), The association of continental crust rocks with ophiolites in the Northern Apennines (Italy): Implications for the continent-ocean transition in the Western Tethys, *Tectonophysics*, *292*(1/2), 43–66, doi:10.1016/S0040-1951(98)00060-2.

McCrea, J. M. (1950), On the isotopic chemistry of carbonates and a paleotemperature scale, *J. Chem. Phys.*, *18*, 849–857, doi:10.1063/1.1747785.

Micklethwaite, S., and S. F. Cox (2006), Progressive fault triggering and fluid flow in aftershock domains: Examples from mineralized Archean fault systems, *Earth Planet. Sci. Lett.*, *250*, 318–330, doi:10.1016/j.epsl.2006.07.050.

Moore, G. F., et al. (2001), New insights into deformation and fluid flow processes in the Nankai Trough accretionary prism: Results of ocean drilling program Leg 190, *Geochem. Geophys. Geosyst.*, *2*, 1058, doi:10.1029/2001GC000166.

Moore, J. C., and D. Saffer (2001), Updip limit of the seismogenic zone beneath the accretionary prism of southwest Japan: An effect of diagenetic to low-grade metamorphic processes and increasing effective stress, *Geology*, *29*(2), 183–186, doi:10.1130/0091-7613(2001)029<0183:ULOTSZ>2.0.CO;2.

Moore, J. C., and P. Vrolijk (1992), Fluids in accretionary prisms, *Rev. Geophys.*, *30*(2), 113–135, doi:10.1029/92RG00201.

Okamoto, S., G. Kimura, and H. Yamaguchi (2006), Earthquake fault rock including a coupled lubrication mechanism, *eEarth Discussions*, *1*, 135–149.

O'Neil, J. R., R. N. Clayton, and T. K. Mayeda (1969), Oxygen isotope fractionation in divalent metal carbonates, *J. Chem. Phys.*, *51*, 5547–5558, doi:10.1063/1.1671982.

Petit, J. P., and E. Laville (1987), Morphology and microstructures of hydroplastic slickensides in sandstone, in *Deformation of Sediments and Sedimentary Rocks*, edited by M. E. P. Jones and R. M. F. Preston, pp. 107–121, Geological Society, London.

Pialli, G., M. Barchi, and G. Minelli (Eds.) (1998), *Results of the CROP 03 Deep Seismic Reflection Profile, Memorie della Società Geologica Italiana*, vol. 52, 657 pp., Società Geologica Italiana, Roma, Italy.

Pini, G. A. (Ed.) (1999), *Tectosomes and Olistrostromes in the Argille Scagliose of the Northern Apennines, Italy*, 70 pp., Geol. Soc. of Am., Boulder, Colo.

Ramsay, J. G. (1980), The crack-seal mechanism of rock deformation, *Nature*, *284*, 135–139, doi:10.1038/284135a0.

Ramsay, J. G., and M. I. Huber (1983), *The Techniques of Modern Structural Geology*, vol. 1, Academic, London.

Ranero, C. R., I. Grevemeyer, H. Sahling, U. Barckhausen, C. Hensen, K. Wallmann, W. Weinrebe, P. Vannucchi, R. von Huene, and K. McIntosh (2008), Hydrogeological system of erosional convergent margins and its influence on tectonics and interplate seismogenesis, *Geochem. Geophys. Geosyst.*, *9*, Q03S04, doi:10.1029/2007GC001679.

Remitti, F. (2005), *Insights into Deformation of Subduction Channels: Ancient Examples From Northern Apennines of Italy and South Island of New Zealand*, 177 pp., Univ. of Modena and Reggio Emilia, Modena, Italy.

Remitti, F., G. Bettelli, and P. Vannucchi (2007), Internal structure and tectonic evolution of an underthrust tectonic mélange: The Sestola-Vidiciatico tectonic unit of the Northern Apennines, Italy, *Geodin. Acta*, *20*, 37–51, doi:10.3166/ga.20.37-51.

Reutter, K., P. Giese, and H. Closs (1980), Lithospheric slip in the descending plate: Observations from the Northern Apennines, *Tectonophysics*, *64*, T1–T9, doi:10.1016/0040-1951(80)90254-1.

Reutter, K.-J., I. Heinitz, and R. Ensslin (1992), Structural and geothermal evolution of the Modino-Cervarola unit, *Mem. Carta Geol. Ital.*, *46*, 257–266.

Ricci Lucchi, F. (1986), The oligocene to recent foreland basins of the Northern Apennines, in *Foreland Basins*, *Int. Assoc. of Sedimentol. Spec. Pub.*, vol. 8, edited by A. Alien and P. Homewood, pp. 105–139, Blackwell, Oxford U. K.

Sadofsky, S. J., and G. E. Bebout (2004), Field and isotopic evidence for fluid mobility in the Franciscan complex: Forearc paleohydrogeology to depths of 30 kilometers, *Int. Geol. Rev.*, *46*, 1053–1088, doi:10.2747/0020-6814.46.12.1053.

Saffer, D. M. (2003), Pore pressure development and progressive dewatering in underthrust sediments at the Costa Rican subduction margin: Comparison with Northern Barbados and Nankai, *J. Geophys. Res.*, *108*(B5), 2261, doi:10.1029/2002JB001787.

Saffer, D. M., M. B. Underwood, and A. W. McKiernan (2008), Evaluation of factors controlling smectite transformation and fluid production in subduction zones: Application to the Nankai Trough, *Isl. Arc*, *17*(2), 208–230, doi:10.1111/j.1440-1738.2008.00614.x.

Sage, F., J. Y. Collot, A. Calahorrano, and P. Charvis (2004), Crustal structure at the Ecuador active margin: Effects of the Carnegy Ridge and associated sea-mounts subduction, *Geophys. Res. Abstr.*, *6*, 05172.

Sahling, H., D. G. Masson, C. R. Ranero, V. Hühnerbach, W. Weinrebe, I. Klaucke, D. Bürk, W. Brückmann, and E. Suess (2008), Fluid seepage at the continental margin offshore Costa Rica and southern Nicaragua, *Geochem. Geophys. Geosyst.*, *9*, Q05S05, doi:10.1029/2008GC001978.

Sample, J. C., M. R. Reid, H. J. Tobin, and J. C. Moore (1993), Carbonate cements indicate channeled fluid-flow along a zone of vertical faults at the deformation front of the Cascadia Accretionary Wedge (Northwest United States Coast), *Geology*, *21*(6), 507–510, doi:10.1130/0091-7613(1993)021<0507:CCICFF>2.3.CO;2.

Screaton, E. J., and D. M. Saffer (2005), Fluid expulsion and overpressure development during initial subduction at the Costa Rica convergent margin, *Earth Planet. Sci. Lett.*, *233*, 361–374, doi:10.1016/j.epsl.2005.02.017.

Sibson, R. H. (2000), Fluid involvement in normal faulting, *J. Geodyn.*, *29*(3–5), 469–499, doi:10.1016/S0264-3707(99)00042-3.

Sibson, R. H. (2001), Seismogenic framework for hydrothermal transport and ore deposition, *Soc. Econ. Geol. Rev.*, *14*, 25–50.

Silver, E., M. Kastner, A. Fisher, J. Morris, K. McIntosh, and D. Saffer (2000), Fluid flow paths in the Middle America Trench and Costa Rica margin, *Geology*, *28*(8), 679–682, doi:10.1130/0091-7613(2000)28<679:FFPITM>2.0.CO;2.

Spinelli, G. A., and M. B. Underwood (2004), Character of sediments entering the Costa Rica subduction zone: Implications for partitioning of water along the plate interface, *Isl. Arc*, *13*(3), 432–451, doi:10.1111/j.1440-1738.2004.00436.x.

Suess, E., G. Bohrmann, R. von Huene, P. Linke, K. Wallmann, S. Lammers, H. Sahling, G. Winckler, R. A. Lutz, and D. Orange (1998), Fluid venting in the eastern Aleutian subduction zone, *J. Geophys. Res.*, *103*(B2), 2597–2614, doi:10.1029/97JB02131.

Swarbrick, R. E., and M. A. Naylor (1980), The Kathikas Melange, S.W. Cyprus—Late cretaceous submarine debris flows, *Sedimentology*, *27*, 63–78, doi:10.1111/j.1365-3091.1980.tb01158.x.

Tavani, M. (2001), Fluid venting and associated processes, in *Anatomy of an Orogen: The Apennines and Adjacent Mediterranean Basins*, edited by G. B. Vai and I. P. Martini, pp. 351–366, Kluwer Acad., London.

Terzi, C., P. Aharon, F. R. Lucchi, and G. B. Vai (1994), Petrography and stable-isotope aspects of cold vent activity imprinted on Miocene age Calcari-a-Lucina from Tuscan and Romagna Apennines, Italy, *Geo-Mar. Lett.*, *14*(2/3), 177–184, doi:10.1007/BF01203729.

Treves, B. (1984), Orogenic belts as accretionary prisms: The example of the Northern Apennines, *Ofioliti*, *9*, 577–618.

Underwood, M. B. (2002), Strike-parallel variations in clay minerals and fault vergence in the Cascadia subduction zone, *Geology*, *30*(2), 155–158, doi:10.1130/0091-7613(2002)030<0155:SPVICM>2.0.CO;2.

Vannucchi, P., and G. Bettelli (2002), Mechanisms of subduction accretion as implied from the broken formations in the Apennines, Italy, *Geology*, *30*(9), 835–838, doi:10.1130/0091-7613(2002)030<0835:MOSAAI>2.0.CO;2.

Vannucchi, P., and L. Leoni (2007), Structural characterization of the Costa Rica decollement: Evidence for seismically induced fluid pulsing, *Earth Planet. Sci. Lett.*, *262*, 413–428, doi:10.1016/j.epsl.2007.07.056.

Vannucchi, P., D. W. Scholl, M. Meschede, and K. McDougall-Reid (2001), Tectonic erosion and consequent collapse of the Pacific margin of Costa Rica: Combined implications from ODP Leg 170, seismic offshore data, and regional geology of the Nicoya Peninsula, *Tectonics*, *20*(5), 649–668, doi:10.1029/2000TC001223.

Vannucchi, P., A. Maltman, G. Bettelli, and B. Clennell (2003), On the nature of scaly fabric and scaly clay, *J. Struct. Geol.*, *25*(5), 673–688, doi:10.1016/S0191-8141(02)00066-4.

Vannucchi, P., F. Remitti, and G. Bettelli (2008), Geologic record of fluid flow and seismogenesis along an erosive subducting plate boundary, *Nature*, *451*, 699–703, doi:10.1038/nature06486.

von Huene, R., and C. R. Ranero (2003), Subduction erosion and basal friction along the sediment-starved convergent margin off Antofagasta, Chile, *J. Geophys. Res.*, *108*(B2), 2079, doi:10.1029/2001JB001569.

von Huene, R., C. R. Ranero, and P. Vannucchi (2004), Generic model of subduction erosion, *Geology*, *32*(10), 913–916, doi:10.1130/G20563.1.

Vrolijk, P., S. R. Chambers, J. M. Gieskes, and J. R. O'Neil (1990), Stable isotope ratios of interstitial fluids from the Northern Barbados accretionary prism, ODP Leg 110, in *Proceedings of the Ocean Drilling Program, Scientific Results, No. 110*, edited by J. C. Moore and A. Mascle, pp. 189–205, Ocean Drilling Program, College Station, Tex.

Wei, W., M. Kastner, and A. Spivack (2008), Chlorine stable isotopes and halogen concentrations in convergent margins with implications for the C1 isotopes cycle in the ocean, *Earth Planet. Sci. Lett.*, *266*(1/2), 90–104, doi:10.1016/j.epsl.2007.11.009.

Zattin, M., A. Landuzzi, V. Picotti, and G. Zuffa (2000), Discriminating between tectonic and sedimentary burial in a foredeep succession, Northern Apennines, *J. Geol. Soc.*, *157*(3), 629–633.

G. Bettelli and F. Remitti, Earth Science Department, University of Modena and Reggio Emilia, Largo S. Eufemia 19, I-41100 Modena, Italy.

C. Boschi and L. Dallai, IGG-CNR, Via Moruzzi, 1, I-56124 Pisa, Italy.

P. Vannucchi (corresponding author), Earth Science Department, University of Florence, Via La Pira 4, I-50121, Firenze, Italy. (paola.vannucchi@unifi.it)